PREDICTIVE NO_X EMISSIONS MODELING FOR A LARGE BORE, LEAN-BURN, INTEGRAL COMPRESSOR ENGINE

A Thesis

by

TAYLOR F. LINKER

Submitted to the Office of Graduate and Professional Studies of
Texas A&M University
in partial fulfillment of the requirements for the degree of

MASTER OF SCIENCE

Chair of Committee,	Timothy J. Jacobs
Committee Members,	Eric L. Petersen
	Adonios N. Karpetis
Head of Department,	Andreas A. Polycarpou

December 2019

Major Subject: Mechanical Engineering

ABSTRACT

The ultimate goal of this work is to aid in the improvement of emissions control methods for compressor engines used in the natural gas transmission pipeline industry. The work presented here contributes to that larger goal by adding onto the capabilities of a previously-developed model of a Cooper-Bessemer GMWH-10C intended to simulate the effects of varying natural gas composition on engine behavior. This work targets the implementation and tuning of NO_x emissions predictions in the engine model, with the expectation that it can be used in the future to inform the development of controller improvements needed for fuel composition variability.

Though the nature of combustion within a lean-burn engine is complex, with many spatial dependencies, the approach taken in this work utilizes a simple 0D/1D, two-zone engine model which lacks rigorous physical accuracy, but produces acceptable engine performance results in a short amount of time. The unique operating conditions of these engines also results in NO_x formation characteristics which are different and more complicated than those in the more common four-stroke, spark-ignited engine commonly used in automotive applications. Thus, special considerations must be taken into account when simulating NO_x formation in a lean-burn engine.

NO_x prediction capabilities were added to the engine model through implementation and assessment of various methods including different pathways of NO_x formation. The best method was tuned to obtain acceptable agreement with experimental data and was tested for its ability to predict emissions for other operating conditions. Finally, a preliminary fuel sweep was performed with the full engine model.

DEDICATION

To my family, friends, and teachers.

ACKNOWLEDGEMENTS

Most importantly, I would like to thank my parents for their unwavering support of everything I have chosen to pursue. They have always set an excellent example for me in all things, big and small. A special thanks to my father for exposing me to the world of engineering from a young age and giving me guidance in my own journey.

Secondly, I would like to thank Dr. Timothy Jacobs for the opportunity to perform research in the AERL. His encouraging attitude and confidence in my abilities have been a consistent driving force for me to continue to push myself. He always has something positive to say or a compliment to pass on about his students' work which never fails to motivate. I am incredibly fortunate for the opportunities I have been given in working with him.

I'd also like to thank Pipeline Research Council International (PRCI) whose support made this work possible. I am especially grateful for the extremely useful technical feedback from Dr. Mark Patterson, Mr. Greg Beshouri, and Mr. Gary Choquette. I would also like to thank Dr. Olivier Mathieu from the Texas A&M Turbomachinery Laboratory for his assistance.

Lastly, but certainly not least, I would like to say thank you to my friends in the AERL. I can only hope find myself in future work environments which are as enjoyable as the one I have experienced while working with you all. A special thanks to Kelsey Fieseler who did a great job at getting me up to speed and provided an excellent model on which to perform my own work.

CONTRIBUTORS AND FUNDING SOURCES

Contributors

This work was supervised by a thesis committee consisting of Professor Timothy Jacobs (advisor) and Professor Eric Petersen of the Department of Mechanical Engineering and Professor Adonios Karpetis of the Department of Aerospace Engineering.

This work utilizes simulations which were developed by others in previous work. Specifically, the GT-Power engine simulation framework was developed by Jake Hedrick and improved on by Kelsey Fieseler. Both are former students who performed their work under Professor Timothy Jacobs. All other work was completed by the student independently.

Funding Sources

Funding for this work was provided by Pipeline Research Council International through contract PR-457-18204. Its contents are solely the responsibility of the authors and do not necessarily represent the official views of Pipeline Research Council International.

NOMENCLATURE

°aTDC	Degrees after top dead center
°bTDC	Degrees before top dead center
BDC	Bottom dead center
BHP	Brake horsepower
CAD	Crank angle degree
C1	Methane, CH_4
C2	Ethane, C_2H_6
C3	Propane, C_3H_8
C4	Butane, C_4H_{10}
C5	Pentane, C_5H_{12}
C5+	Pentane and all higher hydrocarbons
HHC	Heavy hydrocarbon
ID	Ignition delay
IT	Ignition timing
LFS	Laminar flame speed
LoPP	Location of peak pressure
MAE	Mean absolute error
MCC	Main combustion chamber / Main chamber
MN	Methane number
NO	Nitric Oxide
NO_2	Nitrogen dioxide
NO_x	Oxides of Nitrogen, NO and NO_2
OCC	Open combustion chamber / Open chamber
PCC	Pre-combustion chamber / Prechamber
PP	Peak Pressure
PT	Peak temperature
ppm	Parts per million

ppmd	Parts per million, dry basis
ROP	Rate of production
SI	Spark ignition / Spark-ignited
TDC	Top dead center
TER	Trapped equivalence ratio
0D/1D	Zero-dimensional / One-dimensional

TABLE OF CONTENTS

Page

LIST OF FIGURES

Page

LIST OF TABLES

Page

1. INTRODUCTION

1.1. Motivation

While the increase in shale gas production has allowed the United States to meet and even exceed domestic natural gas demand, it has also led to observable fluctuations in the composition of natural gas flowing through the nation's pipelines. Changes in the composition alter the chemical properties of the bulk gas mixture such as its energy density and combustion properties. For pipeline compressor engines, which use the gas as a fuel source, burning abnormal fuel compositions can significantly affect combustion phasing. This can ultimately lead to ramifications such as reduced power output, reduced efficiency, equipment fatigue, and unacceptable emissions levels.

This work is concerned with pipeline engine emissions of oxides of nitrogen (NO_x). Since many pipeline engines in operation today were developed and implemented long before emissions were a primary concern, they have been fitted with many aftermarket technologies to meet increasingly stringent regulations. That said, the implication of fuel variability on NO_x emissions is not fully accounted for by current pipeline engine control systems. Thus, a better understanding of NO_x formation in such engines and reliable methods for predicting engine-out NO_x are both needed to guide the development of technologies which can correct for the fuel-imposed effects.

The study presented here seeks to more completely understand the NO_x formation processes within a pipeline engine. Further, it seeks to develop a reliable but simple NO_x prediction method for use in a full-scale engine model which can reliably capture the effects of fuel composition.

1.2. Background

1.2.1. Natural Gas

Natural gas produced in the United States can be classified in one of three main categories: conventional natural gas, unconventional natural gas, and conventional associated natural gas. Conventional gas is found in large voids between layers of rock and can be extracted via a vertical well drilled into the top of the reservoir. Unconventional gas, often referred to as shale gas or tight gas, occurs in the small spaces within formations of sedimentary rock, such as shale and sandstone, and must typically be extracted using special technologies such as hydraulic fracturing and horizontal drilling. Lastly, conventional associated gas is gas trapped with deposits of crude oil and is, therefore, a byproduct of the oil extraction. [1]

For many decades, conventional natural gas was the primary source for U.S. production, but ultimately declined as it became increasingly difficult for producers to find new conventional resources. Additionally, horizontal drilling and hydraulic fracturing had been around for many decades, but producers had not yet utilized these technologies to extract gas directly from shale resources. These effects lead to a steady reduction in natural gas production in the U.S. after the peak production period in the 1970's. It wasn't until the late 1990's that new improvements to these technologies allowed for economically feasible natural gas production from unconventional resources. This advancement became most noticeable in the U.S. energy markets in the mid-2000's and ultimately lead to the domination of shale-produced gas that is observed today. [2]

The U.S. Energy Information Administration estimates that about 16.86 trillion cubic feet of natural gas was produced from shale resources in 2017. This accounted for about 62% of the total U.S. dry natural gas production in that year alone. [3] Additionally, current projections show this contribution continuing to rise each year in the future. Figure 1 shows how the various natural gas sources stack up to equal the total dry natural gas production history and projections before and after 2018, respectively. The figure shows the best assessment of projections (left) as well as projections considering the sensitivity to high or low resources and technology (center and right). From this, it is noted that the projected tight/shale gas contribution accounts for nearly 40 trillion cubic feet (around 90%) of dry natural gas production by 2050. [4]

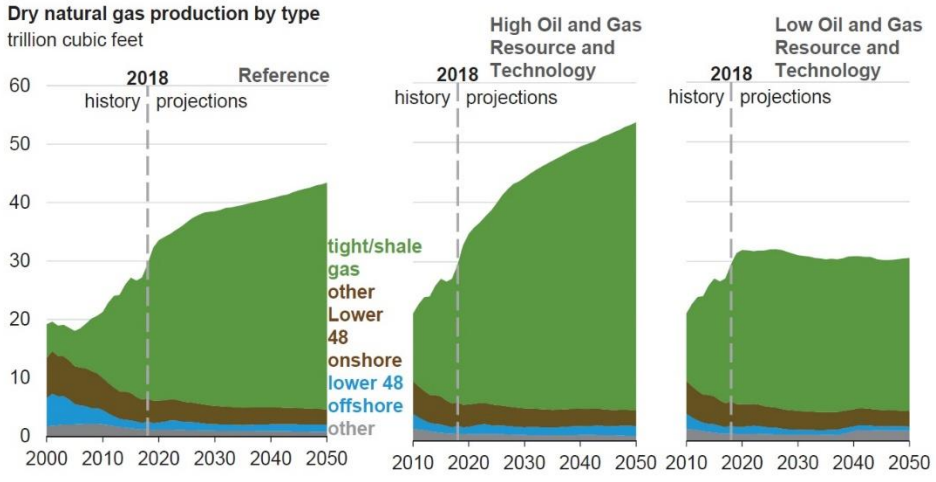

Figure 1: (Left) Total U.S. natural gas production history and projections separated by source. (Center) Assuming high resources and technology. (Right) Assuming low resources and technology. Reprinted from [4].

1.2.2. Natural Gas Composition and Variability

Natural gas is made up of light alkane species (methane (C1), ethane (C2), propane (C3), butane (C4), pentane (C5), etc.) with the mixture primarily consisting of methane. Some natural gas, particularly unprocessed gas, also contains non-trivial concentrations of non-hydrocarbon species such as CO_2, N_2, H_2, and H_2S. Species like CO_2 and N_2 are non-combustible and decrease the heating value of the natural gas mixture; thus, gas processing removes these species among other undesirable components. [5] [6] While conventional natural gas usually holds well to the high methane fraction, gas produced from shale has shown to vary widely in composition. [7]

A study by Choquette [5] highlights the extreme compositional variability that can exist within pipelines. The study analyzed 6,330 gas compositions from interstate pipelines to obtain general statistics about gas speciation and properties. Shown in Table 1, the statistics reveal the large volume fractions that can be achieved by species which usually remain at small or negligible amounts. Perhaps most surprising is the maximum value of ethane, at one point accounting for 100% of the mixture.

Table 1: Gas composition statistics including speciation and bulk gas properties. Adapted from [5].

	HHV (BTU/SCF)	LHV (BTU/SCF)	C2(%)	C4+(%)	CO_2(%)	N_2(%)	H_2(%)
Max	2567	2362	100.00	17.97	50.00	16.81	30.00
Min	749	675	0.00	0.00	0.00	0.00	0.00
Average	1041	939	5.07	0.14	0.56	1.73	0.01

A collection of natural gas composition data taken at a pipeline location in 2016, discussed by Fieseler [8], provides additional insight to how the composition of natural gas changes over time. Figure 2 shows the mole percentages of methane and ethane on an hourly basis, over a nine month period. Noting the different axes but the same linear scales, it is observed from this figure that the concentrations of methane and ethane have a strong inverse trend. Figure 3, on the other hand, shows that propane is relatively insensitive to changes in the volume fractions of other constituents. [8]

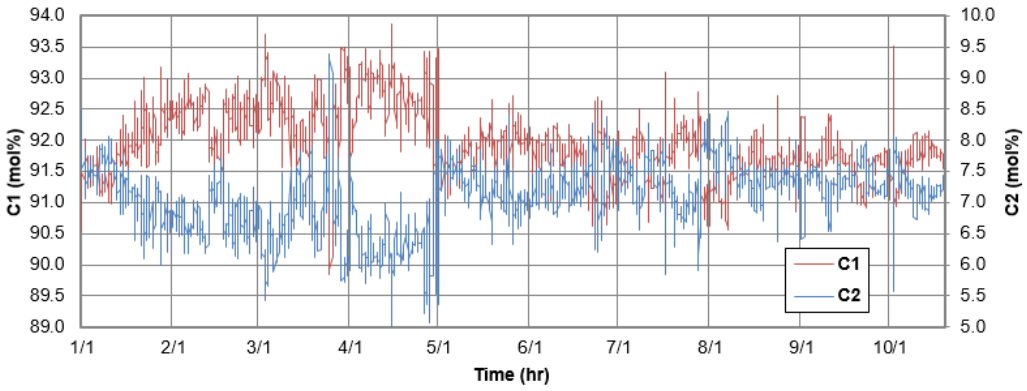

Figure 2: Time-resolved percentages of C1 and C2. Reprinted from [8].

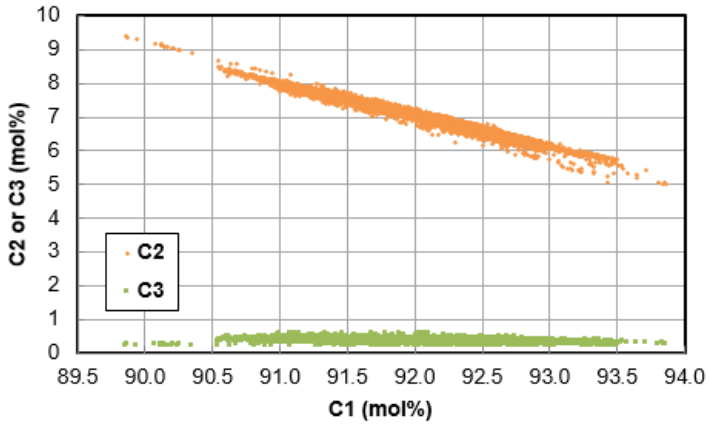

Figure 3: C2 and C3 mole percentage versus C1. Reprinted from [8].

1.2.3. Pipeline Infrastructure and Equipment

The United States natural gas transmission system consists of over 305,000 miles of interstate and intrastate pipelines made up by more than 210 pipeline systems. [9] These wide-diameter, high-pressure main lines connect the areas where gas is produced and processed to storage facilities or distribution centers. From these locations, the gas makes its way to consumers through smaller, low-pressure distribution lines. In 2017, the U.S. Energy Information Administration reported that this network delivered 25 trillion cubic feet of natural gas to 75 million customers. [10]

Compressor stations are located along the pipelines and house compressor units which provide the necessary gas pressure needed to overcome fluid friction losses and keep the gas moving. Stations are typically placed every 50 to 100 miles apart, depending on elevation changes. A variety of prime movers are used to provide the power for compression, though spark-ignited (SI), reciprocating engines are most common. Currently, the natural gas pipeline industry operates roughly 5,600 spark-ignited, gas-fueled engines collectively generating over 9 million brake horsepower (BHP). These engines operate with either a four-stroke cycle or two-stroke cycle. [11] A map of U.S. compressor station locations is shown in Figure 4.

Among the types of reciprocating engines used at compressor stations, the lean-burn, two-stroke integral compressor engine is the most ubiquitous, accounting for approximately 70% of the entire fleet, as of 2005. [11] These engines utilize a small amount of natural gas from the pipeline as a fuel source and provide compression via compressor cylinders integrated directly into the crankcase. As seen in Figure 5, a

typical integral compressor engine has horizontal, double-acting compressor piston/cylinders connected to the crank via a master connecting rod. Power pistons are oriented in a “vee” configuration vertically and attach to the compressor master rod via articulated connecting rods. The simple design and relatively low speed of these engines allows them to attain very long lifespans. In fact, many of the lean-burn, two-stroke integral compressor engines in operation today are “legacy” units between 30 and 60 years old; some of these are expected to run for at least another 40 years. [12]

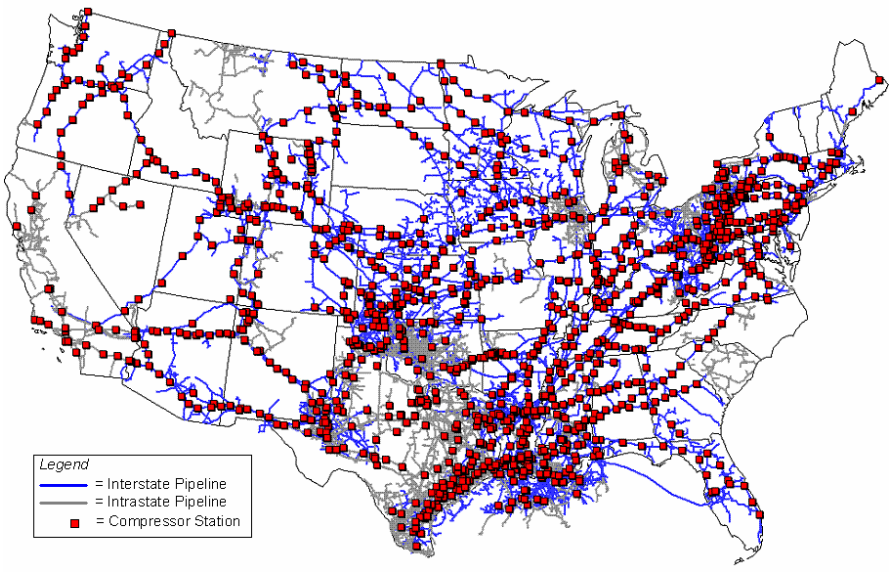

Figure 4: U.S. natural gas pipelines and compressor stations as of 2008. Reprinted from [13].

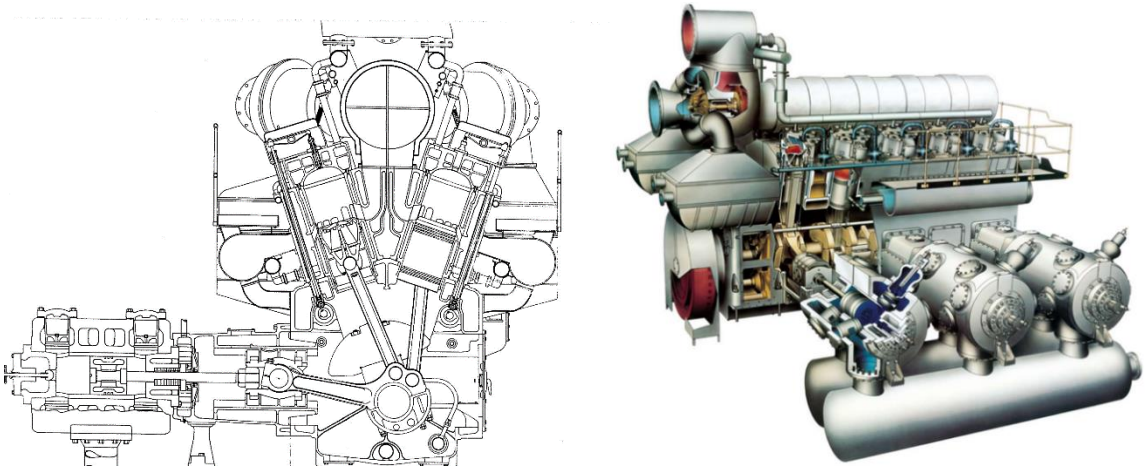

Figure 5: Cross-section and isometric views of an integral compressor engine. Reprinted from [12].

1.2.4. The Two-Stroke Cycle Engine

1.2.4.1. Cycle Processes

For reciprocating internal combustion engines, a piston/cylinder connected to a crank shaft is used as the means by which to convert the energy released from combustion of the fuel into useful shaft work. Though this is common across all reciprocating internal combustion engine platforms, the cycle used to produce power may be different. It is on this basis that the two-stroke engine is different from that of the four-stroke engine typically utilized in automotive applications. In a two-stroke engine, two strokes of the piston (one revolution of the crankshaft) are required to achieve one power-output event or power stroke. This is compared to a four-stroke engine which requires four strokes of the piston (two revolutions of the crankshaft) per power stroke.

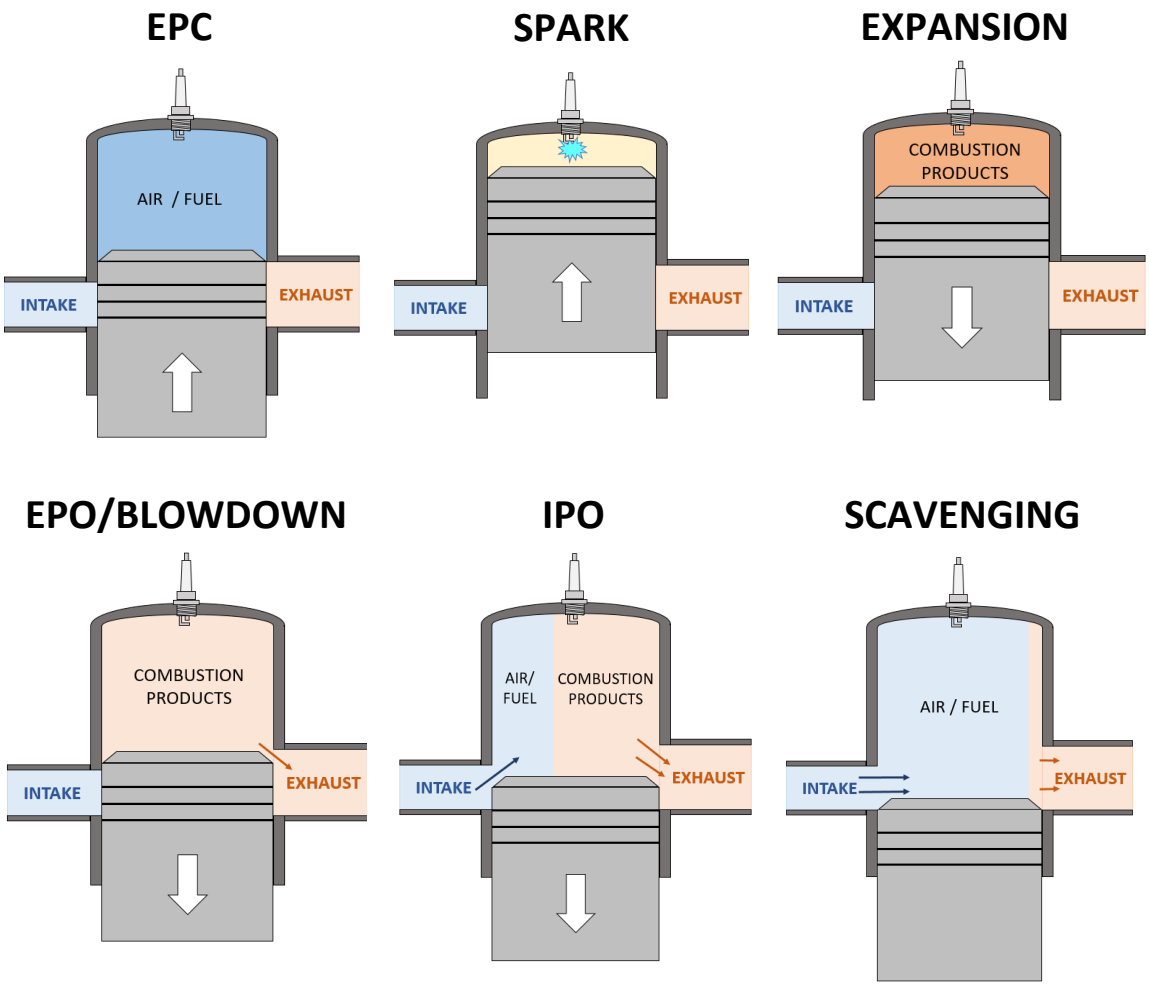

Figure 6: Illustration of two-stroke cycle processes.

The processes of the spark-ignited two-stroke cycle are illustrated in Figure 6 and will be explained here. The cycle begins at exhaust port closing (EPC) when the cylinder is sealed off and contains a fixed amount of trapped mass. The piston continues to rise, compressing the gases until top dead center (TDC) at which point the cylinder is at its minimum volume. Just before TDC, the spark plug discharges, providing energy to ignite the fuel/air mixture. The subsequent heat released during combustion causes the cylinder gases to expand, pushing the piston back down, producing power. Towards the end of the expansion stroke, the piston reaches the point of exhaust port opening (EPO)

which allows the high pressure exhaust gases to exit the cylinder during blowdown. Shortly after this point, intake port opening (IPO) allows fresh air (and fuel, if premixed) to enter the cylinder while gases are still being exhausted. This simultaneous intake and exhaust process is referred to as scavenging. The piston continues to descend toward the point of maximum volume at bottom dead center (BDC), and continues back up toward intake port closing (IPC) when no new gases can enter the cylinder.

1.2.4.2. Open Chamber versus Pre-Chamber Engines

Two-stroke engines may differ in the way the cylinder is designed to ignite the fuel/air mixture and carry out the combustion process. Many two-stroke engines are designed with an open combustion chamber (OCC), or open chamber, utilizing a spark plug located directly in the cylinder. This type of construction was displayed in Figure 6 and is also the primary design used for four-stroke automotive engines.

For large bore, lean-burn natural gas engines, using a precombustion chamber (PCC), or prechamber, is a common method used to effectively reduce NO_x emissions. A prechamber is a small chamber, usually 1-2% of the cylinder clearance volume, attached to the main chamber (MCC) where the piston is located. In the PCC, a stoichiometric fuel/air mixture is created with a fuel injector and is then ignited by a conventional spark plug, initiating combustion. Pressure rise within the PCC pushes the igniting mixture into the MCC, igniting the fuel and air located there. [14] The burning jet that is propelled to the main chamber can have an ignition energy approximately one million times greater than that of a standard a standard spark plug. Hence, the PCC helps

to extend the lean limit of the engine by allowing for a much leaner fuel/air mixture in the MCC which can be ignited by the burning jet. Since fuel/air equivalence ratio greatly affects the presence of NO_x in engine exhaust, discussed in detail in section 2.2, the overall leaner operation of the engine helps to reduce NO_x emissions. [15] Figure 7 depicts the typical construction of a prechambered cylinder.

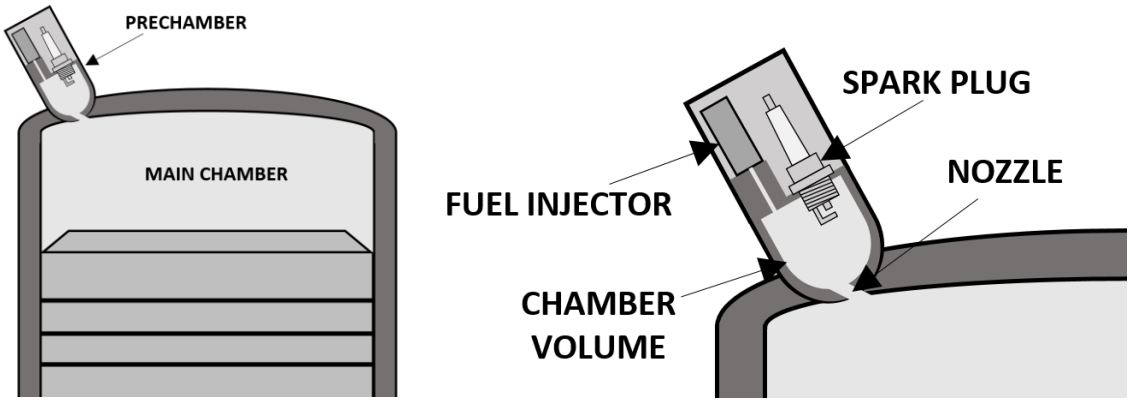

Figure 7: Typical cylinder in a prechambered engine.

1.2.5. Oxides of Nitrogen

Oxides of nitrogen are taken to primarily include nitric oxide (NO) and nitrogen dioxide (NO_2) and are collectively referred to as NO_x. They are one of five main classes of pollutant species emitted from combustion sources; other classes include carbon monoxide, organic compounds, sulfur oxides, and particulates. [16] The combustion process catalyzes the formation of NO_x species by providing sufficient energy and chemical feedstock needed for the production of NO.

For hydrocarbon combustion, it has been found that NO forms through four primary reaction mechanisms; namely, the extended Zeldovich (thermal) mechanism, the

nitrous oxide (N_2O) mechanism, the prompt mechanism, and the NNH mechanism. [17] Each mechanism contributes differently to the total NO formed depending on the specific combustion conditions. Further reactions of the produced NO may then form NO_2 under favorable conditions. The formation of NO_x species is discussed extensively in sections 2.2 through 2.4.

1.2.5.1. Health and Environmental Impacts

NO_2 is regulated by the Environmental Protection Agency since it is the most predominant form of NO_x formed by human activity. Not only is NO_2 a pollutant itself, posing a direct respiratory hazard to humans, but it also plays a role in the formation of tropospheric ozone and acid rain. [18] [19]

The role which NO_2 plays in forming ozone (O_3) can be described by reactions (1) and (2). In reaction (1), NO_2 is irradiated with ultraviolet light, resulting in atomic oxygen which participates in reaction (2) with molecular oxygen to form ozone. [20] The NO produced from reaction (1) can then react again with radical species to form NO_2, repeating the process. In this way, NO molecules can be recycled repeatedly in the production of ozone. [21] NO_2 in the atmosphere may also react with water via reaction (3) to form nitric acid (HNO_3). When combined with rainwater, the resulting acidic solution makes its way back to earth where it can harm crops, humans, animals, or erode infrastructure, among other adverse results. [22]

$$NO_2 + h\nu \rightleftarrows NO + O \quad (1)$$

$$O + O_2 + M \rightleftarrows O_3 + M \quad (2)$$

$$3NO_2 + H_2O \rightleftarrows 2HNO_3 + NO \quad (3)$$

NO does not have as much of a direct impact as NO_2, but also contributes to the hazards discussed above by reacting to form NO_2. Reactions (4) through (6) are some primary atmospheric reactions by which NO results in NO_2. The lifespan of NO in the atmosphere before conversion to NO_2 is short, lasting just minutes, if not seconds. In reaction (5), R represents an organic group, such as methyl. [23]

$$2NO + O_2 \rightleftarrows 2NO_2 \quad (4)$$

$$NO + RO_2 \rightleftarrows NO_2 + RO \quad (5)$$

$$NO + O_3 \rightleftarrows NO_2 + O_2 \quad (6)$$

1.2.5.2. NO_x Regulations for Pipeline Engines

NO_x regulations for new lean-burn, two-stroke compressor engines are defined by the New Source Performance Standards which sets standards for all criteria pollutants emitted from new stationary engines. Lean-burn engines manufactured after July, 2010 must meet a level of 1.0 g/BHP-hr. [24] For grandfathered engines, such as the one considered in this work, NO_x regulations fall to the state or regional level; however, the 1.0-2.0 g/BHP-hr range is also common among these regulations. In terms of volumetric exhaust concentration, as is used for simulation validation in this work, 2 g/BHP-hr for a

typical lean-burn pipeline engine corresponds roughly with an exhaust concentration value of 100-200 ppmd (parts per million on a dry basis). Retrofitted technologies allow for normal operation much below regulation levels, as low as 0.15-0.2 g/BHP-hr in some cases. These values correspond to NO_x concentrations as low as 10-20 ppmd. [25]

1.3. Objective

The objective of this work is to incorporate reliable NO_x emissions prediction capabilities into the existing engine simulation of a Cooper-Bessemer GMWH-10C integral compressor pipeline engine. This work aims to arrive at a prediction method which can obtain reasonable NO_x predictions which align well with experimental data, and can ultimately capture the effect of fuel composition variability.

2. LITERATURE REVIEW

2.1. Engine Combustion Modeling

Engines are often simulated with either quasi-dimensional thermodynamic models or multi-dimensional models. Multi-dimensional engine simulations are more complex and are based on governing partial differential equations. These models are intended to capture the physical and chemical processes in the cylinder, allowing them to retain more physical accuracy which gives the user insight to the complex processes in the real engine. The spatial considerations also provide more accurate emissions predictions, but the use of multi-dimensional models is often time consuming. Quasi-dimensional simulations invoke a sense of dimensionality in their construction, but do not have any mathematical link to the spatial context of the cylinder. These models are less physically accurate and often require plenty of empirical data to tune into agreement with real engine behavior; however, once tuned, they provide quick and sufficiently accurate predictions for engine performance and emissions. [26] A quasi-dimensional model is considered and used in this work.

One type of quasi-dimensional thermodynamic SI engine simulation uses a two-zone methodology. This method splits the cylinder volume into an unburned gas zone and a burned gas zone, providing a sense of the dimensionality of flame propagation combustion in an SI engine. During the simulated combustion period, a small amount of fuel and air mass is transferred from the unburned zone to the burned zone at each time step and combustion is carried out. The thermodynamic properties of the zones and are

calculated and the simulation continues. The rate at which mass is transferred between zones can either be prescribed with a Wiebe function or can be determined predictively throughout combustion by considering more fundamental combustion properties such as laminar flame speed. [26] [27] Figure 8 provides a simple diagram of a two-zone model.

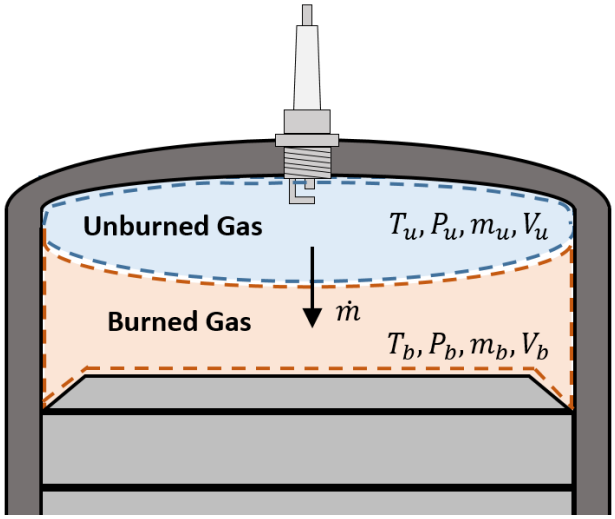

Figure 8: Schematic of spark-ignited, two-zone simulation methodology.

It is common to simulate the concentrations of combustion product species and temperature in the burned zone by assuming chemical equilibrium. This approach is usually sufficient since the reactions which form the primary products of combustion are extremely quick, eliminating the need for complex, rate-controlled chemistry. [26]

2.1.1. GT-Power Engine Modeling

One commercial software which utilizes a quasi-dimensional approach for SI engine simulation is GT-Power, a 0D/1D solver developed by Gamma Technologies. This software offers users the capability to simulate many engine configurations using

basic sub-models (cylinders, piping, injectors, etc.) which are connected together to represent the entire engine system. GT-Power utilizes simple models for heat transfer, friction, gas exchange, and emissions, but users have the option to modify/tune these models or create their own, offering more flexibility. [28] [29]

In GT-Power's two-zone, SI, turbulent flame combustion model, chemical equilibrium of the burned zone is calculated by assuming 13 products of combustion: N_2, O_2, CO_2, CO, H_2O, H_2, H, O, OH, NO, N, SO_2 (if fuel sulfur is present), and Ar (inert). Once the equilibrium composition is calculated, the internal energy of the burned zone is determined. Using the energy equations in (7) and (8), the unburned and burned zone temperatures as well as the cylinder pressure are calculated at each time step.

$$\frac{d(m_u e_u)}{dt} = -p\frac{dV_u}{dt} - Q_u + \left(\frac{dm_f}{dt}h_f + \frac{dm_a}{dt}h_a\right) + \frac{dm_{f,i}}{dt}h_{f,i} \qquad (7)$$

$$\frac{d(m_b e_b)}{dt} = -p\frac{dV_b}{dt} - Q_b - \left(\frac{dm_f}{dt}h_f + \frac{dm_a}{dt}h_a\right) \qquad (8)$$

Subscripts u and b refer to the unburned and burned zones, respectively. Subscript a refers to air, f refers to fuel, and f, i refers to the fuel injected. Also, m is mass, e is specific energy of the zone, p is cylinder pressure, V is the volume of the zone, Q is the rate of heat transfer from the zone, and h is enthalpy. [29]

The GT-Power two-zone, SI combustion model is utilized in this work for the prediction of NO_x emissions. Further information on the specific model is discussed later in section 3.2.

2.2. NO Formation Pathways

The presence of NO within engine exhaust is dependent on many factors, but is strongly driven by the fuel/air equivalence ratio within the cylinder. The plot from Heywood [27] in Figure 9 shows how several exhaust pollutant species, including NO, change qualitatively with operating equivalence ratio. The trends show that NO concentration peaks just on the lean side of stoichiometric at an equivalence ratio of about 0.95 and drastically falls off as the mixture is either richened or leaned from that point.

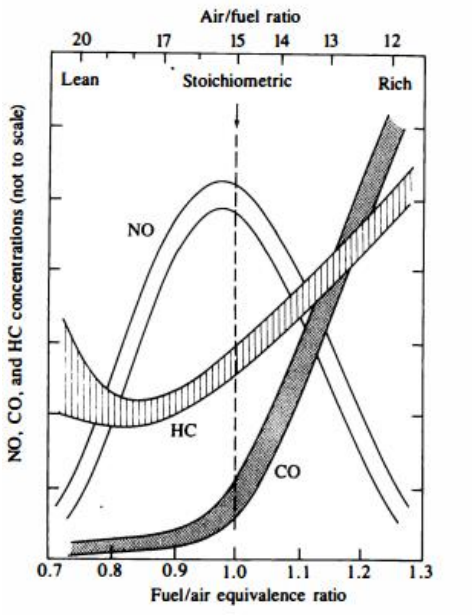

Figure 9: Variation of several exhaust pollutant species as engine fuel/air equivalence ratio changes. Reprinted from [27].

The formation mechanisms which drive this behavior will be discussed in the following subsections. A discussion of other parameters such as temperature and pressure and their effects on NO production is also provided.

2.2.1. Extended Zeldovich (Thermal) Pathway

Perhaps the most well-known NO formation pathway is the thermal pathway described by the extended Zeldovich mechanism. This three-reaction mechanism, given by reactions (9) through (11), is generally considered the primary source of NO formation for the combustion of near-stoichiometric fuel/air mixtures. [27] Hence, the peak seen in Figure 9 is primarily attributed to the extended Zeldovich reactions. Reactions (9) and (10) were originally proposed by Zeldovich [30] and Lavoie et al. [31] added reaction (11) to the mechanism due to its nontrivial contribution to NO formation for certain conditions.

$$O + N_2 \rightleftarrows NO + N \tag{9}$$

$$N + O_2 \rightleftarrows NO + O \tag{10}$$

$$N + OH \rightleftarrows NO + H \tag{11}$$

The NO formed through this mechanism is commonly referred to as thermal NO due to the strong temperature dependence of reaction (9). Since this reaction requires a large amount of energy to break the triple-bond of the molecular nitrogen, it requires sufficiently high temperatures and acts as a rate-limiting step for the mechanism. [26] This reaction's dependence on high temperatures is so strong that, as a general rule, the extended Zeldovich mechanism is rather inactive at temperatures below 1800 K. [32] The near-stoichiometric peak seen in Figure 9 is mainly driven by, and roughly aligns with, the behavior of flame temperature as fuel/air equivalence ratio is varied, as seen in

Figure 10. The peak of NO concentration exists in the slightly lean region due to the larger presence of molecular and atomic, dissociated oxygen which the mechanism also favors through reactions (10) and (11). Formation of thermal NO is rather slow compared to the timescales of combustion. It is for this reason that thermal NO is considered to form primarily in the post-flame gases, decoupling its formation from the combustion process. [6] [26]

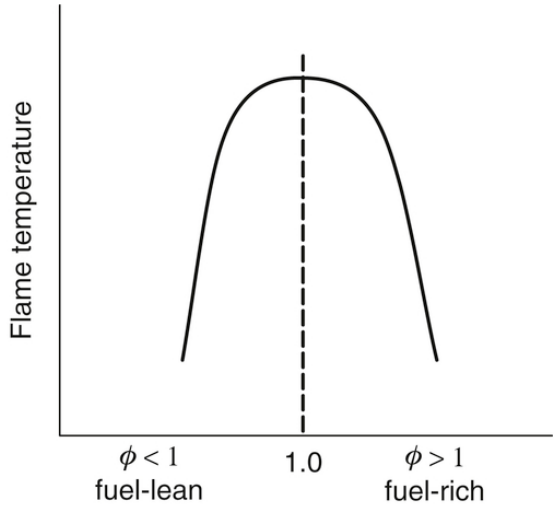

Figure 10: Behavior of flame temperature versus fuel/air equivalence ratio. Reprinted from [20].

In reciprocating engines, the initially burnt gases are further compressed and heated by the energy release of subsequently burning fuel. This additional temperature rise helps to drive the production of the thermal NO.

2.2.2. Nitrous Oxide (N_2O) Pathway

The nitrous oxide, or N_2O, mechanism discussed by Malte and Pratt [33] is another important NO_x formation pathway for particular combustion conditions. This mechanism is initiated by a three-body, recombination reaction with molecular nitrogen and atomic oxygen to form the intermediate N_2O species, as shown in reaction (12). The N_2O molecule then proceeds to react with other species, resulting in the conversion back to N_2 via reactions (13) and (14), or in the formation of NO via reaction (15). [33] Other sources also indicate that N_2O results in NO through reaction (16). [17] [34] [35]

$$N_2 + O + M \rightleftarrows N_2O + M \quad (12)$$

$$N_2O + H \rightleftarrows N_2 + OH \quad (13)$$

$$N_2O + O \rightleftarrows N_2 + O_2 \quad (14)$$

$$N_2O + O \rightleftarrows NO + NO \quad (15)$$

$$N_2O + H \rightleftarrows NO + NH \quad (16)$$

The N_2O mechanism is found to be most important for lean, low temperature, high pressure conditions. At such conditions, the thermal NO contribution will be suppressed and the high pressures will promote the forward reaction rate of reaction (12) due to its three-body dependence. [26] The effect of increasing pressure on the nitrous oxide mechanism is discussed in work by Drake and Blint [36] in which an increase in reaction pressure from 0.1 atm to 20 atm resulted in an increase in production from the mechanism from 3% to 20% of total NO_x. Other sources also suggest that the

contribution from the mechanism can be significant in conditions were intense mixing is present. [16]

2.2.3. Prompt Pathway

In experiments by Fenimore [37], it was found that some NO was formed in the primary reaction zone of hydrocarbon flames; a location where extended Zeldovich reactions would not be active enough to form NO due to the short time scale. Fenimore proposed that this quickly-formed, or "prompt", NO stems from flame zone radicals which react with molecular nitrogen to form intermediate species such as amines or cyano compounds. These intermediates then react with other species and eventually result in the formation of NO. The flame zone reactions thought to be most responsible for the initiation of the prompt NO pathway, or Fenimore mechanism, are given by reactions (17) and (18), where reaction (17) acts as the rate-limiting step. [32]

$$CH + N_2 \rightleftarrows HCN + N \tag{17}$$

$$C + N_2 \rightleftarrows CN + N \tag{18}$$

Work by Lavoie and Blumberg [38] concluded that NO resulting from the flame zone reactions can be important for rich combustion, or in high-dilution (lean) cases when overall NO production is low. Leonard and Correa [39] also determined that the inclusion of the mechanism was an important contributor to NO_x at low temperatures.

2.2.4. NNH Pathway

The NNH mechanism, originally introduced by Bozzelli and Dean [40], is another pathway by which NO can form and is described by reactions (19) and (20).

$$N_2 + H \rightleftarrows NNH \tag{19}$$

$$NNH + O \rightleftarrows NO + NH \tag{20}$$

The NNH mechanism has been found to be important for premixed and non-premixed flames and for hydrocarbon fuels with large carbon-to-hydrogen ratios. [41] [32] Compared to the other NO formation pathways discussed, the NNH mechanism is relatively new; thus, its applicability at engine conditions has not been studied as extensively. This is also due to the fact that, like other mechanisms, it is negligible compared to the formation of primary, thermal NO in most engines.

2.2.5. Fuel-Bound Nitrogen Pathway

Nitrogen bound to fuel molecules may also contribute to the formation of NO in combustion processes. However, this NO source is only particularly important for fuels such as coal which can have a significant presence of fuel-bound nitrogen (up to 2% by mass). [32] Natural gas contains only unbound, molecular nitrogen in typically trace amounts. Therefore, the formation of NO from fuel nitrogen is nonexistent for pipeline compressor engines and is not considered further in this work.

2.3. NO_2 Formation and Destruction Pathways

Nitrogen dioxide (NO_2) typically comes in much lower concentrations than NO in the exhaust of internal combustion engines. As an example, the plot from Heywood [27] in Figure 11 shows typical NO and NO_2 concentrations found in the exhaust of a SI engine typical in automotive applications. Though this is different than the engine considered in this work, the plot indicates that the peaks of NO and NO_2 presence in the exhaust are not aligned, showing that the peak of NO_2 exists at a higher air/fuel ratio.

Any NO_2 found in the exhaust of an internal combustion engine is formed through the further oxidation of NO. All NO exhausted to the atmosphere will eventually be converted to NO_2 via reactions (4) through (5), discussed in section 1.2.5.1.; however, these reactions are far too slow to be a significant source of engine-out NO_2. [42]

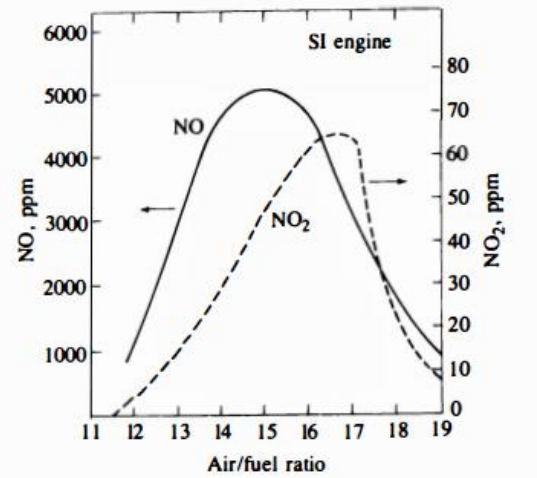

Figure 11: Typical NO and NO_2 concentrations in spark ignited engine exhaust versus air/fuel ratio. Reprinted from [27].

In a study of flat methane/air flames, Merryman and Levy [43] found that the initial appearance of NO_2 occurred very early in the pre-flame reaction zone and increased in concentration through the visible flame zone. This work led to the conclusion that NO_2 is likely formed when HO_2 radicals react with NO via reaction (21).

$$NO + HO_2 \rightleftarrows NO_2 + OH \tag{21}$$

Merryman and Levy also observed that for rich and stoichiometric flames, high temperatures in the post-flame zone cause NO_2 destruction and subsequent conversion back to NO, resulting in a corresponding spike in NO concentration. Kinetic modeling by Tassitano [44] showed that, for engine-relevant conditions, this destruction is most likely to occur through reaction (22); though, at temperatures above 1150 K and in the absence of atomic hydrogen, reaction (23) could also be important. Reaction (23) agrees with the conversion of NO_2 to NO suggested by Heywood.

$$NO_2 + H \rightleftarrows NO + OH \tag{22}$$

$$NO_2 + O \rightleftarrows NO + O_2 \tag{23}$$

The destruction of NO_2 at high temperatures explains the general trends observed in Figure 11. Since, in most engines, all of the burned gases make it to the high post-flame temperatures, little NO_2 is left behind to be exhausted to the atmosphere. Though, while this may be true for open chamber, spark-ignited engines, the complex combustion

processes within a large bore, lean-burn, prechambered engine allows for much higher NO_2/NO_x ratios. Often times, these ratios can reach unity for extremely lean operation.

2.4. Engine-Specific NO_x Considerations

2.4.1. Spark Timing

The spark timing of the engine significantly affects engine NO_x emissions and its role is well understood. As spark timing advances, combustion occurs earlier within the cycle leading to more heat release near or before TDC, this advances the location of peak pressure (LoPP) making for higher in-cylinder pressures and in-cylinder temperatures. The increase in temperature results in higher thermal NO production leading to more engine-out NO_x. Retarding the spark timing has the opposite effect. [27]

2.4.2. Prechamber Contribution to NO_x

Prechambers help to reduce overall engine NO_x emissions by allowing an engine to operate at much leaner equivalence ratios than are possible for an open chamber configuration. However, in a study by Olsen and Lisowski [45], it was found that the PCC itself is responsible for a significant part of the NO_x which is formed in a lean-burn, prechambered engine. In that study, the engine was operated first with two PCCs, then with one PCC. Results showed that dual PCC operation had roughly 42% higher NO_x emissions than the single PCC. However, the study also found that PCC NO_x levels were lower than those measured in the exhaust. This led to the conclusion that PCCs contribute to NO_x emissions via the jet of burning fuel and air which they expel into the

main chamber. The high temperature gases in the jet drive the production of thermal NO_x, leading to a high NO_x contribution. The remainder of MCC combustion then contributes lower NO_x amounts. These physical processes are depicted in Figure 12.

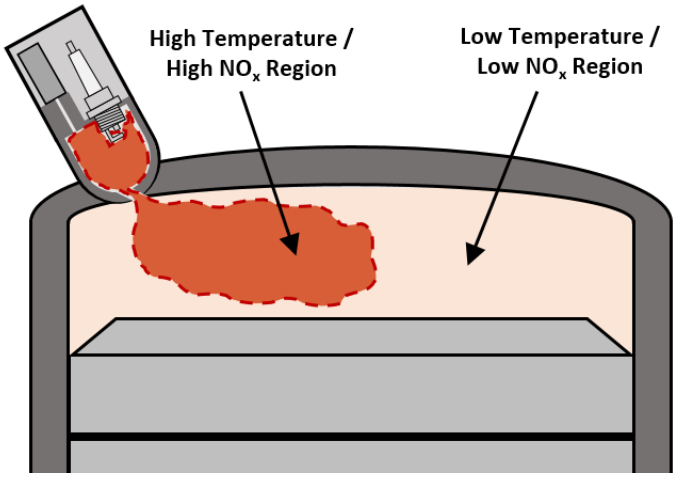

Figure 12: Prechamber gas plume contribution to exhaust NO_x. Adapted from [45].

The extent to which a PCC contributes to total exhaust NO_x is dependent on many factors including PCC volume fraction relative to MCC volume at TDC, compression ratio, PCC and MCC equivalence ratios, speed, and load. [46] Though this variability leads to different specific PCC contributions across different engines, it is widely recognized that the PCC contributes to a majority of total the NO_x in lean-burn engines. [15] Results from a lean-burn, four-stroke, natural gas engine studied by Gringrich et al. [47] showed that the PCC contributed 10% of total NO_x at the recommended operating point, but upwards of 75% at the engine's lean limit. The PCC NO_x further increased as its equivalence ratio was richened. Hiltner and Loetz [46] also

found a significant PCC NO_x contribution from a lean-burn research engine; between 60% and 70% of total NO_x for most normal operating conditions.

2.4.3. NO_2 Survival

Generally speaking, the ratio of NO_2 to NO is small, if not zero, for the exhaust of stoichiometric engines. However, this does not extend to lean-burn natural gas engines which can have large NO_2/NO ratios, particularly at lean conditions. In fact, for many cases in which overall exhaust NO concentrations are below 50 ppm, NO_2/NO ratios can exceed 1. [48] This behavior can be attributed to several aspects regarding the unique operation of prechambered, lean-burn engines.

One reason driving the large survival of NO_2 is the relatively small effect that leaning has on NO_2 relative to NO formation. Though NO is a precursor for NO_2, a decrease in NO from leaning does not result in a proportional decrease in NO_2. This is because higher levels of NO inhibit the production of HO_2 radicals which are used in reaction (21) to form NO_2. This then explains why leaning the fuel/air mixture to lower NO emissions allows for relatively more NO_2 formation, resulting in higher NO_2/NO ratios. [48]

Another contributor to the large presence of exhaust NO_2 is the existence of quenching regions within the cylinder which do not reach high enough temperatures to facilitate the destruction of NO_2 back to NO via reactions such as (22) and (23). One such region could occur in the location where the flame zone is extinguished before complete combustion can take place, leaving untouched fuel and air or partial-

combustion products. This may be due to a pocket of fuel and air which is too lean to ignite, or in a small crevice within the cylinder which is too small for the flame to enter. A thin volume near the cylinder wall which experiences higher local heat loss may also act as a quenching region. Engine modeling by Tassitano [44] showed that crevice volumes and wall quenching can account for the lion share of exhaust NO_2 in a large bore, natural gas engine, in some cases as much as 80% of the total.

Hilliard and Wheeler [49] noted that the high-stratification in diesel engines allows for NO_2 to be blown from the flame zone and into cooler cylinder pockets which act as quenching regions, leading to higher exhaust NO_2. This is different from homogeneous, premixed gasoline engines which have smaller low-temperature zones, leading to lower exhaust NO_2 and higher NO. [49] The same effect of stratification on NO_2 is likely at play in prechambered natural gas engines. Any NO_2 formed in the prechamber gases could be blown into quenching zones, resulting in more exhaust NO_2.

2.5. Engine NO_x Modeling

Compared to the primary products of combustion like CO_2 and H_2O, accurately simulating the formation of NO_x species within engines is more difficult and requires a greater level of attention. This is due to the dependency of NO_x formation on the nature of the combustion process and the slower timescales of NO formation reactions. Thus, chemical equilibrium is not sufficient for calculating NO concentration when simulating NO_x formation at engine conditions. [26] Engine modeling results by Caton, in Figure

13, show how the instantaneous equilibrium concentration of NO (labeled NO_{eq}) are significantly different than the real concentration (labeled NO) during combustion.

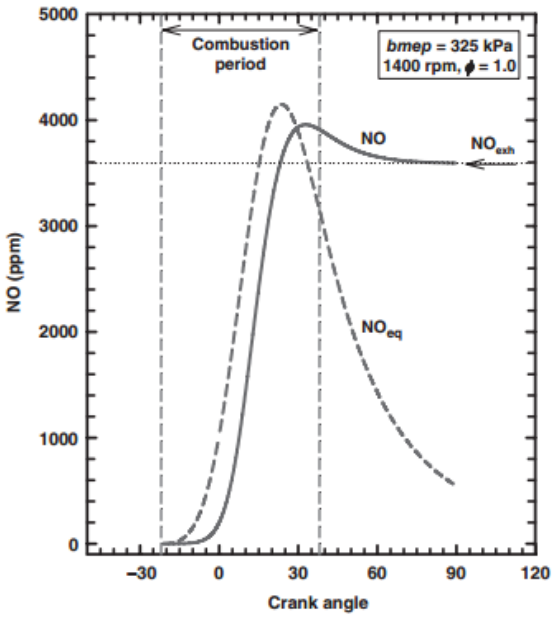

Figure 13: In-cylinder NO concentration predicted with equilibrium chemistry and reaction kinetics. Reprinted from [26].

The inadequacy of equilibrium chemistry for NO_x predictions calls for the use of reaction kinetics with NO mechanisms which more accurately capture the time dependency of NO formation. The rate of each reaction is represented by a rate coefficient determined by the Arrhenius form given in equation (24).

$$k = AT^b \exp\left(-\frac{E_A}{R_u T}\right) \tag{24}$$

Here, A is the pre-exponential factor in cm^3/mol-s, b is the temperature exponent, E_A is the activation energy in cal/mol, T is temperature in K, and R_u is the universal gas constant in cal/mol-K. [32]

The most ubiquitous approach to modeling NO_x emissions for internal combustion engines is with the use of the extended Zeldovich mechanism alone. This approach is usually taken because of the overwhelming contribution of thermal NO for combustion conditions typical of most SI engines with little or no NO formed through other mechanisms. Thus, considering only extended Zeldovich reactions results in a decent NO_x prediction for most SI engines. Further, the extended Zeldovich mechanism works well with the equilibrium combustion approach, allowing for NO_x predictions with small computational expense. [27]

Considering all three reactions of the extended Zeldovich mechanism, the rate of formation of NO can be found with equation (25). Here, the rate coefficient subscripts *1*, *2*, and *3* indicate the reaction in the mechanism and subscripts *f* and *r* indicate whether the rate coefficient is for the forward or reverse direction.

$$\frac{d[NO]}{dt} = k_{1f}[O][N_2] + k_{2f}[N][O_2] + k_{3f}[N][OH] - k_{1r}[NO][N] - k_{2r}[NO][O] - k_{3r}[NO][H] \quad (25)$$

Using equilibrium concentrations of O, O_2, OH, H, and N_2 and assuming a steady state N concentration, as discussed by Heywood [27], results in a greatly simplified rate of NO formation.

Numerous engine modeling studies have used the extended Zeldovich mechanism alone to predict NO formation. Since many such models target the NO_x emissions of stoichiometric, four-stroke engines, use of the extended Zeldovich mechanism produces results in excellent agreement with experimental data. [50]

Raine et al. [51] discussed the selection of rate data to be used with the extended Zeldovich mechanism for use in SI engine simulations. These authors evaluated several sets of rate data suggested throughout literature and found that very different predictions of exhaust NO can be obtained depending on the set used. Some authors have tuned published, experimentally-determined rate data in order to arrive at a better match with experiments. For example, Lavoie and Blumberg [52] used extended Zeldovich mechanism rate data from the work by Baulch et al. [53] but adjusted the rate constant for k_1 downward by 35% to obtain better agreement with experimental values.

Pirker et al. [54] used the extended Zeldovich mechanism alone to model NO_x formation in a GT-Power model of a large, prechambered natural gas engine. The authors accounted for fluid motion between the MCC and PCC, allowing for greater accuracy in NO concentrations. Results in that work were not compared rigorously against experimental data to judge quantitative accuracy with real emissions data. Similarly, Hiltner and Loetz [46] used GT-Power to simulate NO_x formation in a prechambered natural gas engine. These authors also accounted for NO transfer between PCC and MCC, but also included the $N_2O+O \rightarrow NO+NO$ reaction from the N_2O mechanism along with the three extended Zeldovich reactions. Primary products of

combustion, such as those used by the extended Zeldovich mechanism, were obtained with equilibrium. It is not entirely clear how the concentration of N_2O was determined.

Several other authors have shown that the consideration of thermal NO alone is not enough to account for all exhaust NO_x for lean SI engines. In work by Lavoie et al. [31] the N_2O mechanism was included in addition to the extended Zeldovich mechanism in a quasi-dimensional model of an engine running at leaner conditions. The N_2O mechanism showed to contribute nontrivially to total NO_x as equivalence ratios decreased to 0.8. A larger contribution from extended Zeldovich reactions was observed for equivalence ratios of 1 and higher.

Based on the work by Fenimore [37] discussed earlier, Moore [55] suggested that the contribution of prompt NO can be roughly determined by equation (20). Here, $f(ER)$ represents a certain function dependent on the fuel/air equivalence ratio, P is pressure, and $[NO\ equil]_{AFT}$ is the concentration of NO when equilibrium is attained at the adiabatic flame temperature of the mixture at the given pressure.

$$Prompt[NO] = f(ER) * P^{\frac{1}{2}} * [NO\ equil]_{AFT} \tag{26}$$

Dodge et al. [56] used this equation, fitted with an equivalence ratio function determined by Corr et al. [57], as part of a NO_x formation subroutine in the model of an open chamber, lean-burn, natural gas engine operating at equivalence ratios as low as 0.6. These authors found that the addition of the equation improved the agreement of engine-out NO_x predictions with experimental data, particularly for the leanest operating

conditions which were under predicted with thermal NO alone. For operating conditions with equivalence ratios higher than 0.75, thermal NO contributions began to dominate, with prompt NO contributions changing negligibly. That said, the authors did note that the prompt correlation given by equation (20) may also be including the contribution of NO formed through the N_2O mechanism. Since the N_2O mechanism emerged after Fenimore's work, the NO first attributed to prompt reactions alone may have been formed, in part, by N_2O pathway reactions. Thus, the correlation used by Dodge et al. may have over predicted the actual contribution of prompt NO for those engine conditions. [56]

In work by Pundle [58] all NO formation mechanisms were included in the model of a prechambered, large bore, lean-burn, natural gas engine by using a full natural gas combustion mechanism. This model included significant detail by dividing the cylinder into unburned, burned, and flame front gases, each represented by a different chemical reactor with prescribed residence times. MCC and PCC were not considered separately in that model, but the prechamber was characterized by a richer sub-zone of the unburned gas zone. In the leanest case investigated in that work (430% theoretical air), the N_2O mechanism accounted for nearly 40% of the engine-out NO_x, with the rest coming primarily from the extended Zeldovich reactions. Both prompt and NNH pathways showed to be weak contributors to engine-out NO_x. That work resulted in simplified NO formation rate equations for NO formed through thermal and N_2O pathways where N_2O is assumed to be in equilibrium and forms NO through reactions with O and H.

Other work by Pundle et al. [34] used the same quasi-dimensional model framework to simulate an open chamber, large bore, lean-burn natural gas engine. In this simulation, only thermal and N_2O pathways were considered. Results showed that around 30% of NO_x was formed via the nitrous oxide mechanism at equivalence ratios below 0.6 (above $\lambda \approx 1.7$); the contribution of the mechanism increased with decreasing equivalence ratio (increasing λ).

2.6. Variable Fuel Composition Effects

As mentioned earlier, variations in natural gas composition cause changes in the gas's heating value and reactivity. Reactivity is a general term used here to describe the propensity of a fuel to combust under certain conditions, as well as how quickly combustion progresses. Two particularly important metrics by which the reactivity of a fuel/air mixture can be characterized are through laminar flame speed and ignition delay.

2.6.1. Laminar Flame Speed

The speed at which the reaction zone, or flame, propagates through a premixed fuel/air mixture is described by the flame speed. When reactants enter the flame or are engulfed by the flame in laminar flow conditions, the velocity of the flame with respect to the reactants is called the laminar flame speed (LFS). Though combustion takes place in a turbulent flow field in a SI engine cylinder, the LFS of the fuel/air mixture is still an important property which, in part, dictates the rate at which combustion will occur. [27]

The presence of larger chain hydrocarbons in natural gas, such as ethane, works to increase the LFS of the mixture. This phenomena is caused by the presence of hydrogen and enhanced radicals which form during the combustion of these lower H/C ratio hydrocarbons. The participation of such reactive species quickens the combustion process. [59]

Fieseler [8] carrier out a sensitivity study using the LFS dataset to understand the relative impact that different variables have on LFS. The results of this study are presented in Table 2. The percent positive and negative values indicate the likelihood that an increase in the respective variable will cause an increase or decrease in the laminar flame speed, respectively. Thus, the results of the study show that mixture properties such as temperature, pressure, and equivalence ratio have the largest effect on LFS. A nontrivial sensitivity to fuel species composition is also observed, particularly for methane and ethane. Propane and heavier hydrocarbons have a weaker impact.

Table 2: Sensitivity study for LFS with respect to mixture properties and fuel composition. Adapted from [8].

Variable	Sensitivity	Percent Positive	Positive Magnitude	Percent Negative	Negative Magnitude
Pressure	0.576	0	0	100	0.5763
Equiv. Ratio	0.555	90	0.5954	10	0.1883
Temperature	0.4012	100	0.4012	0	0
Res. Fraction	0.0226	0	0	100	0.0226
Methane	0.2211	0	0	100	0.2211
Ethane	0.1908	100	0.1908	0	0
Propane	0.0205	100	0.0205	0	0
Butane	0.0071	100	0.0071	0	0
Pentane	0.0065	100	0.0065	0	0

2.6.2. Ignition Delay

Ignition delay (ID) describes the amount of time it takes for a fuel/air mixture to combustion at certain thermodynamic conditions. While a simple definition, the quantitative measurement of ID can be significantly different depending on what is taken to be the start of combustion; a definition which varies across fields and applications. When experimentally measured in shock tubes or rapid compression machines, ID references a start of combustion defined by the initial peak of radical species such OH. In spark-ignited engines, such as the pipeline engines considered in this work, the extreme local conditions developed by the spark plug result in a start of combustion basically coinciding with spark timing. Therefore, ID in engines is often referred to as the time until a small, but insignificant, amount of fuel mass has burned, usually within 1% to 5%. [7]

Much like LFS, ID is also affected by the presence of hydrocarbons larger than methane. Since C-C bonds, as found in ethane and larger, required less energy to break apart than C-H bonds, larger amounts of heavier hydrocarbons (HHCs) result in decreased ignition delay time. Methane is made up entirely up C-H bonds which makes its ID time much longer. [59]

The same study by Fieseler [8] also studied the sensitivity of ID with respect to thermodynamic properties and fuel composition. Results are shown in Table 3. The sensitivity of ID to independent fuel species is not as readily observed in this study since the fuel dependency is represented by methane number (MN). However, an increased amount of HHCs results in a lower MN.

Table 3: Sensitivity study for ID with respect to mixture properties and fuel composition. Adapted from [8].

Variable	Sensitivity	Percent Positive	Positive Magnitude	Percent Negative	Negative Magnitude
Temperature	4.77	0	0	100	4.77
Pressure	1.12	0	0	100	1.12
Equiv. Ratio	0.4012	0	0	100	0.076
MN	0.0399	100	0.0399	0	0
Res. Fraction	0.00449	100	0.00449	0	0

2.6.3. Engine Operation

As discussed in the previous sections, changes in the composition of natural gas affect combustion properties such as LFS and ID. The end results of increased fuel reactivity are similar to that of a more advanced spark timing. In essence, more heat is released earlier, higher in-cylinder peak pressures are attained, and in-cylinder temperatures increase resulting in more NO formation. Several studies have shown these results for a broad range of small, spark-ignited, natural gas engines. [60] [61] [62]

The effect of fuel reactivity on two-stroke, large bore, lean-burn, engine operation and NO_x emissions was observed in a study by Ladd et al. [63] which held engine operating condition relatively constant while the amount of fuel ethane was increased from 5% to 20%. In-cylinder pressure traces from this study are shown in Figure 14 and show quicker combustion occurring with larger ethane fraction. This is evident from the advance in location of peak pressure and the increase in peak pressure. NO_x emission values across the ethane sweep showed to increase by roughly 1 g/BHP-hr, resulting in levels which were out of compliance for the engine.

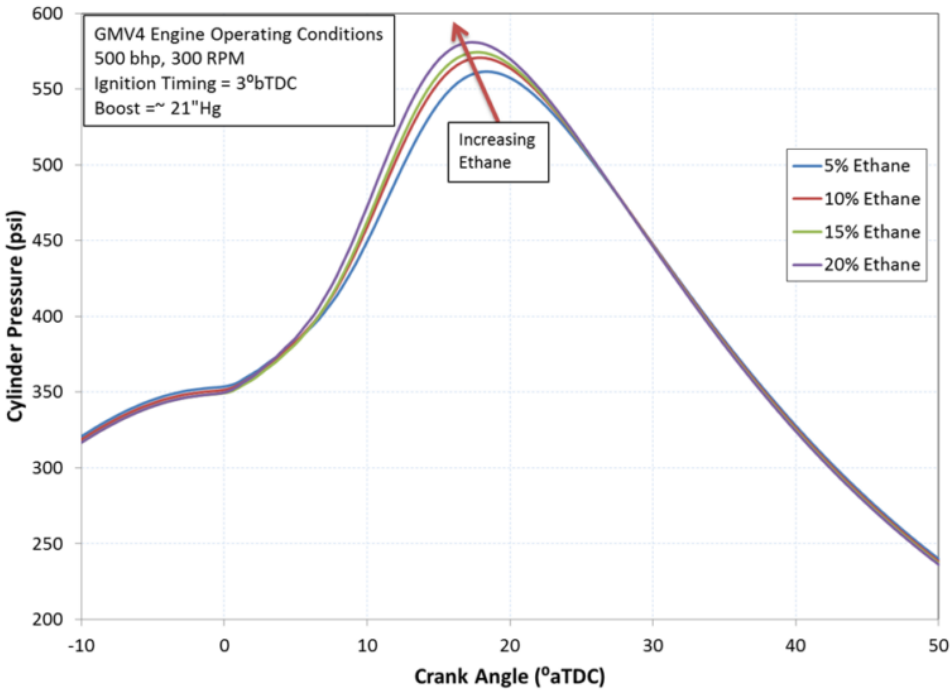

Figure 14: In-cylinder pressure traces as fuel ethane percentage is increased showing advancement in LoPP and higher peak pressures. Reprinted from [63].

3. EXPERIMENTAL DATA & MODEL DESCRIPTION

3.1. Field Engine Data Collection

Data used for this work was taken from an in-field Cooper-Bessemer GMWH-10C integral compressor pipeline engine. In total, 17 operating conditions were tested which varied in equivalence ratio, ignition timing (IT), and torque. Engine speed was kept constant at 250 rpm which is characteristic of typical engine operation. This data was collected as part of a previous project phase which used the data to validate a full-scale engine model of the engine of interest. [8] The GMWH is shown in Figure 15 and its specifications are listed in Table 4.

Figure 15: Cooper-Bessemer GMWH-10C used for data collection.

Table 4: Engine specifications

Make	Cooper-Bessemer
Model	GMWH-10C
Cycle	Two-Stroke
Rated HP	3,400
Rated Speed (rpm)	250
Number of Cylinders	10
Cylinder Configuration	Prechamber (2 per cylinder)
Configuration	V-bank
Bore (inches)	18
Stroke (inches)	20

Operating condition measurements collected included speed, manifold temperatures, manifold pressures, air flow rate, fuel flow rate, turbocharger speed, fuel composition, and ambient conditions. These measurements, and basic knowledge of the engine geometry can be used to calculate what is referred to as the trapped equivalence ratio (TER), which is a measure of the effective global engine equivalence ratio. The TER adjusts the approximation of fuel/air equivalence ratio from bulk mass flows to account for the aspects of operating condition which may affect the actual in-cylinder equivalence ratio at port closure. This parameter is used in the TER control method which has been used for pipeline engine control for the past 20 years. [12] The torque of the engine is calculated on a percentage-basis of rated engine torque (71,427 lbf-ft) and IT is given in terms of degrees before top dead center (°bTDC) and has a nominal value of 3.5 °bTDC for this engine.

Exhaust emissions data includes values for O_2, CO, total hydrocarbons (THC), NO, and NO_2. NO_x species were recorded on a parts per million, dry basis (ppmd). The 17 runs and their respective TER, IT, torque, NO, and NO_2 values are given in Table 5.

It is noted that all NO_x emissions came in the form of NO_2 except for the two richest cases, Run-15 and Run-16. This data demonstrates the large NO_2/NO_x ratios that are typical for large bore, lean-burn, prechambered engines, as discussed in section 2.4.3. It should also be mentioned that Runs 15 and 16, while within reasonable NO_x regulation levels, are rather uncharacteristic of this engine's normal operation, with NO_x values being ~10x larger than the other 15 runs in which are more representative.

Table 5: Summary of operating points tested and respective NO/NO_2 emissions.

	TER	IT (°bTDC)	Torque (%)	NO (ppmd)	NO_2 (ppmd)
Run-1	0.399	3.5	76	0.0	7.8
Run-2	0.403	3.5	86	0.0	9.5
Run-3	0.400	3.0	83	0.0	8.3
Run-4	0.410	3.5	91	0.0	11.5
Run-5	0.405	4.0	91	0.0	12.9
Run-6	0.409	4.5	91	0.0	14.4
Run-7	0.410	5.0	90	0.0	15.5
Run-8	0.407	3.5	88	0.0	10.5
Run-9	0.410	3.0	89	0.0	11.2
Run-10	0.421	2.5	90	0.0	11.4
Run-11	0.408	3.5	96	0.0	14.3
Run-12	0.401	3.5	91	0.0	10.4
Run-13	0.378	3.5	90	0.0	9.7
Run-14	0.421	3.5	90	0.0	19.1
Run-15	0.466	3.5	91	115.0	22.9
Run-16	0.470	3.5	92	143.0	22.8
Run-17	0.401	2.0	84	0.0	8.0

Since the engine data was collected over a short, two-day span, the fuel composition across the runs were very similar and revealed little to no changes in the mole fractions of methane, ethane, or propane. Nonetheless, the exact compositions were recorded and used in all engine modeling work utilizing the dataset.

3.2. Engine Model Description

This work improves on the full-scale engine model of the Cooper-Bessemer GMWH-10C mentioned in the previous section. This model was created as part of the Master's thesis work of Fieseler [28] which aimed to develop a detailed pipeline engine model that could predictively modify combustion characteristics to account for fuel composition changes. Though the real engine has PCCs, this model represents the engine as having OCC construction. The lack of initial ignition energy that the PCCs would provide are made up for with an enlarged simulated spark size which quickens the flame kernel growth. This approach resulted in acceptable agreement with experimental data. The model was validated for performance with the experimental data discussed earlier, but NO_x emissions predictions and accuracy were not attempted. Further, the lack of natural gas variability in the experimental data did not allow for the validation of model performance under variable fuel cases. [28]

Specific details about GT-Power, the GMWH model, and model validation can be found in the cited thesis by Fieseler [28], but the aspects which are most relevant to this work will be discussed next.

3.2.1. Combustion

The GMW model in this work uses a two-zone, predictive, spark-ignition, turbulent flame combustion model. This model is intended for simulating homogeneous charge, spark-ignited engines and is predictive in the sense that the burn rate is calculated throughout combustion based on in-cylinder properties, as opposed to being prescribed based on a Wiebe function in a non-predictive model. [29]

The amount of mass transferred from the unburned zone to the burned zone in each simulation time step is dictated by the burn rate calculated in equation (27). This equation is dependent on the unburned mass entrained (M_e) and a time constant (τ) which are each determined through equations (28) and (29), respectively.

$$\frac{dM_b}{dt} = \frac{M_e - M_b}{\tau} \tag{27}$$

$$\frac{dM_e}{dt} = \rho_u A_e (S_T + S_L) \tag{28}$$

$$\tau = \frac{\lambda}{S_L} \tag{29}$$

In these equations, M_b is the burned mass, τ is the time constant, M_e is the unburned mixture entrained mass, ρ_u is the density of the unburned mass, A_e is the flame front surface area, S_T is the turbulent flame speed, S_L is the laminar flame speed, and λ is the Taylor microscale length. [29]

The laminar flame speed value used in the model calculated using equations (30) and (31). Coefficients in these equation were expanded by Fieseler [8] to be functions of fuel species mole fractions. Thus, the model is able to adjust the laminar flame speed for fuel composition in addition to temperature, pressure, equivalence ratio, and residual fraction.

$$S_L^o = \left(B_m + B_\phi(\phi - \phi_m)^2\right)\left(\frac{T}{T_{ref}}\right)^\alpha \left(\frac{P}{P_{ref}}\right)^\beta (Dilution) \quad (30)$$

$$Dilution = 1 - 0.75D(1 - (1 - 0.75 * D * X_{res})^7) \quad (31)$$

A similar approach was taken by Fieseler for modeling ID, but the equation was not implemented in the GT-Power due to software limitations. Therefore, the GT-Power model currently only accounts for fuel effects on LFS.

3.2.2. NO_x Emissions

As mentioned in section 3.2.1, GT-Power uses chemical equilibrium to obtain concentrations of 13 product species, including NO, at each simulation time step. However, as discussed in section 2.1, equilibrium concentrations of NO are not reliable. For this reason, GT-Power offers several options for achieving more accurate NO_x predictions.

One method by which NO_x can be predicted in GT-Power is through the use of a built-in extended Zeldovich mechanism subroutine. The mechanism uses reaction rate

coefficients calculated using the Arrhenius form and rate data cited by Heywood [27]. The subroutine is summarized in Table 6.

Table 6: GT-Power extended Zeldovich mechanism subroutine reaction rate coefficients. Adapted from [29].

Reaction	Reaction Rate Coefficient (m^3/kmol-s)
$O + N_2 \rightleftarrows NO + N$	$k_1 = F_1 * 7.60e10 * \exp\left(\frac{-38000 * C_1}{T_b}\right)$
$N + O_2 \rightleftarrows NO + O$	$k_1 = F_2 * 6.40e6 * T_b * \exp\left(\frac{-3150 * C_2}{T_b}\right)$
$N + OH \rightleftarrows NO + H$	$k_3 = F_3 * 4.10e10$

It is noted that emission of nitrogen oxides are reported as "NO_x" when using the subroutine, but no NO_2 formation pathways are included. Overall reaction rate multipliers (F_1, F_2, F_3) and activation energy multipliers (C_1, C_2) are provided to tune the reaction rates so that simulated NO_x values better align with experimental NO_x data. The user also has the option of creating their own NO_x subroutine by prescribing reactions and the respective rate data. [29]

Alternatively, all equilibrium chemistry in the model can be overridden completely by implementing a combustion mechanism for use in governing burned zone kinetics. In this way, reaction kinetics calculations are used to calculate the species concentrations in the burned zone of the model. GT-Power allows for the use of any combustion mechanism constructed in CHEMKIN II format and solves the in-cylinder kinetics with a 3-state, 5th order RADAU ODE solver. Overriding burned zone

equilibrium allows for the most flexibility in predicting NO_x since other NO-forming pathways besides the extended Zeldovich mechanism can be included, in addition to pathways for NO_2 formation. [29]

The work presented in the results of this paper explore these different options for obtaining NO_x in order to arrive at accurate predictions. Results from the various methods helped to guide subsequent approaches at NO_x predictions. These are discussed in section 4.

4. RESULTS: NO_X MODELING IMPLEMENTATION

Implementation of NO_x predictions in the GT-Power model was carried out through several different approaches. In all cases, however, the prediction of NO_x from the model was assessed and tuned based on experimental total NO_x data which shared the same nominal spark timing of 3.5°bTDC. This approach was taken to get a baseline for the performance of the NO_x predictions without the effect of spark timing coming into play. Additionally, all 10 nominal runs have NO_x emissions within regulation values, but the eight leanest runs were used more heavily for assessment. Since Run-15 and Run-16 are much richer than normal engine operation, they were only used in making broad conclusions about the model.

4.1. Extended Zeldovich Mechanism

Initial addition of NO_x predictions to the GT-Power model was achieved with the use of the provided extended Zeldovich mechanism subroutine in the software. As explained in section 3.2.2, this subroutine can be used when combustion is simulated with equilibrium and simply calculates NO via the three reactions of the extended Zeldovich mechanism. These initial results are presented in Figure 16 and Figure 17 where NO_x values are plotted versus the experimental TER. Since some data points have near-equal TER values, data will primarily be presented in the form of Figure 18 which shows NO_x values for each run in the order of increasing TER; this helps to spread the data points for easier inspection.

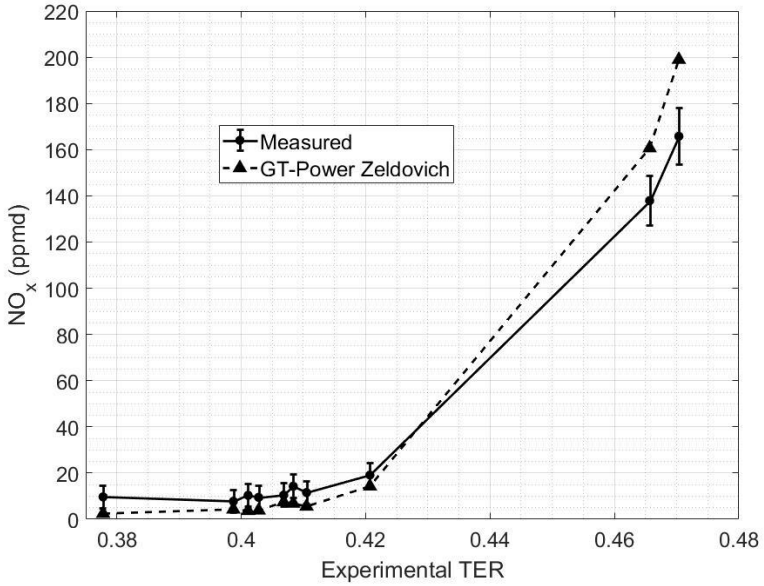

Figure 16: Experimental NO_x and predicted NO_x, versus experimental TER, using GT-Power extended Zeldovich subroutine.

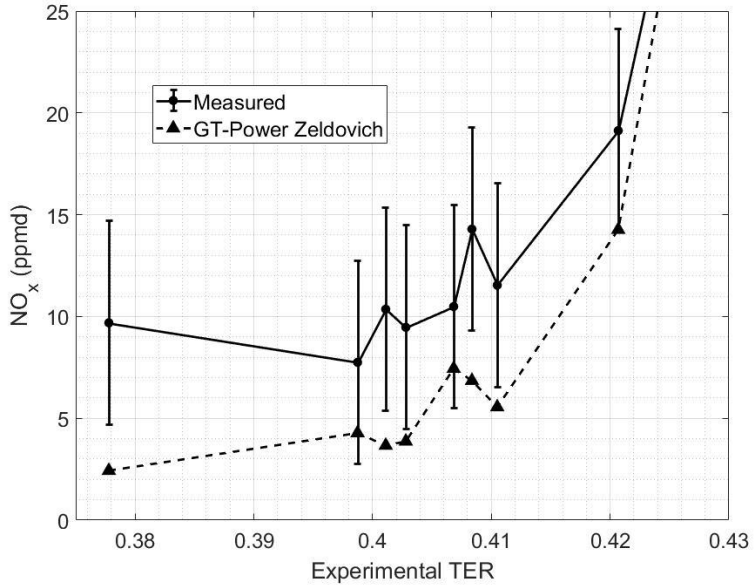

Figure 17: Experimental NO_x and predicted NO_x, versus experimental TER, using GT-Power extended Zeldovich subroutine. 8 leanest cases.

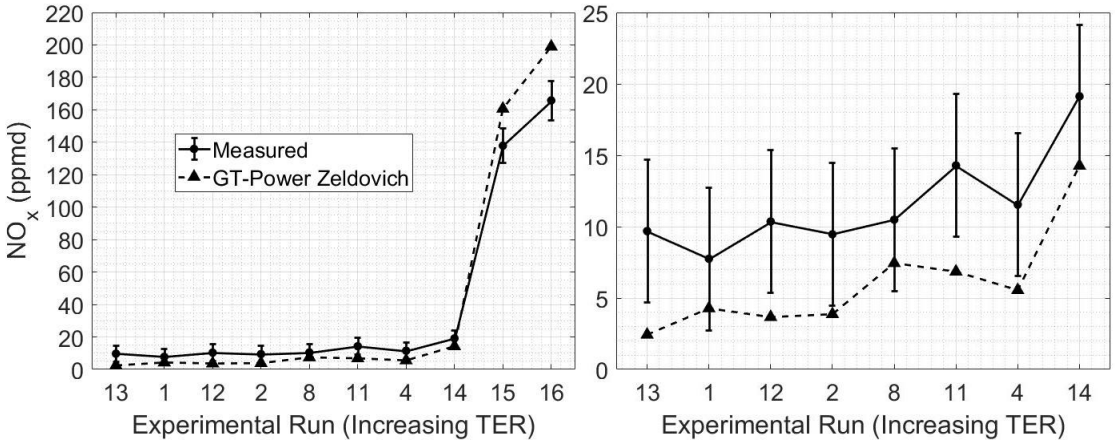

Figure 18: (Left) Experimental NO_x and predicted NO_x, versus experimental run, using GT-Power extended Zeldovich subroutine. (Right) 8 leanest cases.

The results show that NO_x is under predicted for the leanest cases and over predicted for the richest cases when using the extended Zeldovich mechanism. That said, use of the mechanism does capture the trend in exhaust NO_x behavior as equivalence ratio increases. This indicates that the temperatures within the model are behaving appropriately as the conditions become richer.

It is noted that the error in predicted NO_x for the lean cases is quite small on a concentration basis, only being under predicted by an average of ~5.5 ppmd. However, for many of the lean cases, this error amounts to a 50% under prediction or more. The results of Figure 16 through Figure 18 also show that the concentration errors in predicted values are consistently outside of the measurement accuracy. Together, these indicate that, while the extended Zeldovich mechanism alone can capture the general trends in NO_x, improvements could be made to make predictions more accurate.

4.1.1. Extended Zeldovich Rate Data Comparison

NO_x predictions were investigated further with the use of different extended Zeldovich reaction rate data found in literature. As discussed in rate data investigation by Raine et al. [51], different sets of accepted Zeldovich rate data found throughout literature can yield drastically different results when used for predicting NO_x emissions from internal combustion engines. Thus, it was thought that a different set may provide more accurate results than those cited from Heywood. The sets of rate data investigated here originate from Miller and Bowman [64], Hanson and Salimian [65], GRI-Mech2.11 [66], GRI-Mech3.0 [67], Dean and Bozzelli [68], Blumberg and Kummer [50], Lavoie and Blumberg [52], and Glarborg et al. [69]. These sets are summarized in Table 7.

Reaction rate datasets were implemented in GT-Power using a subroutine similar to that tried initially; however, the rate data is supplied to the software in the form of a data file constructed in CHEMKIN format which indicates the species, reactions, and the Arrhenius rate coefficient constants A, b, and E_A. Results when using the various datasets are shown in Figure 19 and Figure 20.

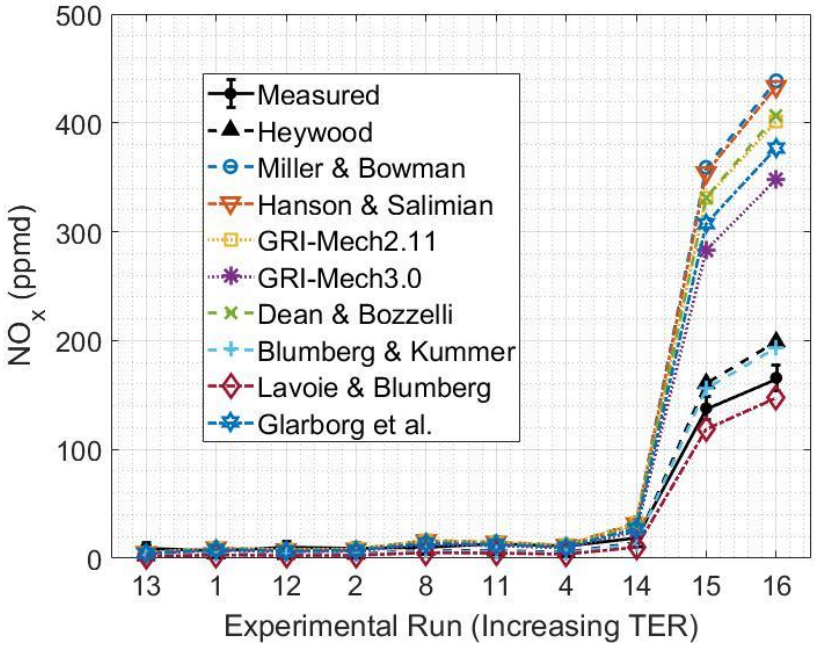

Figure 19: Comparison extended Zeldovich rate datasets found in literature.

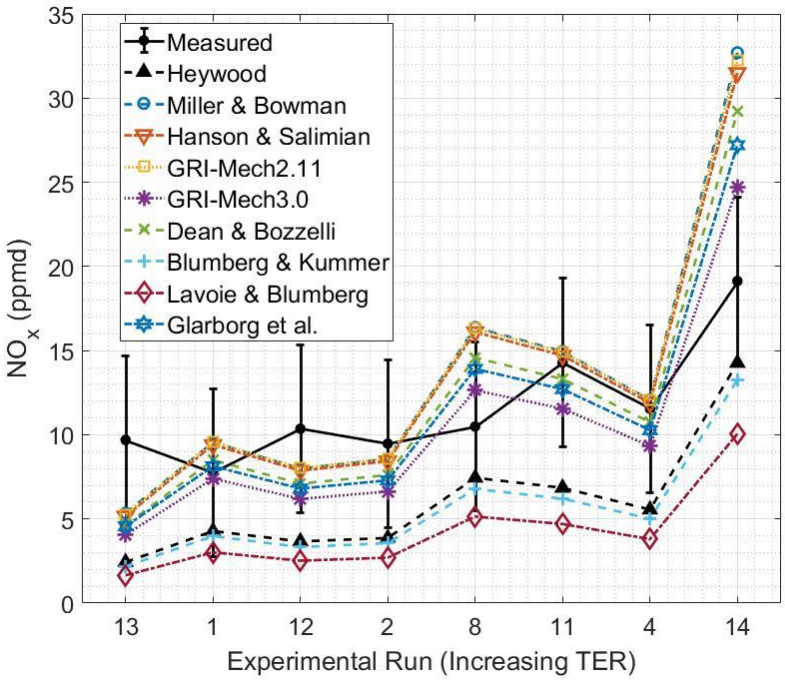

Figure 20: Comparison of extended Zeldovich rate datasets. 8 leanest cases.

Table 7: Investigated sets of extended Zeldovich mechanism rate data.

Authors	Reaction	A (cm^3/mol-s)	b	E_A (cal/mol)
Miller and Bowman	$N+NO \rightarrow N_2+O$	3.27×10^{12}	0.3	0.0
	$N+O_2 \rightarrow NO+O$	6.40×10^{9}	1.0	6279.0
	$N+OH \rightarrow NO+H$	3.80×10^{13}	0.0	0.0
Hanson and Salimian[1]	$N+NO \rightarrow N_2+O$	3.80×10^{13}	0.0	735.0
	$N+O_2 \rightarrow NO+O$	1.60×10^{10}	1.0	8882.0
	$N+OH \rightarrow NO+H$	5.40×10^{13}	0.0	3418.0
GRI-Mech2.11	$N+NO \rightarrow N_2+O$	3.50×10^{13}	0.0	330.0
	$N+O_2 \rightarrow NO+O$	2.65×10^{12}	0.0	6410.0
	$N+OH \rightarrow NO+H$	7.33×10^{13}	0.0	1121.0
GRI-Mech3.0	$N+NO \rightarrow N_2+O$	2.70×10^{13}	0.0	355.0
	$N+O_2 \rightarrow NO+O$	9.00×10^{9}	1.0	6500.0
	$N+OH \rightarrow NO+H$	3.36×10^{13}	0.0	385.0
Dean and Bozzelli	$N+NO \rightarrow N_2+O$	4.11×10^{13}	0.0	1421.0
	$N+O_2 \rightarrow NO+O$	9.0×10^{9}	1.0	6497.0
	$N+OH \rightarrow NO+H$	1.10×10^{14}	0.0	1123.0
Blumberg and Kummer	$N+NO \rightarrow N_2+O$	1.32×10^{13}	0.0	0.0
	$N+O_2 \rightarrow NO+O$	1.81×10^{8}	1.5	5961.0
	$N+OH \rightarrow NO+H$	4.20×10^{13}	0.0	0.0
Lavoie and Blumberg	$N+NO \rightarrow N_2+O$	1.00×10^{13}	0.0	0.0
	$N+O_2 \rightarrow NO+O$	6.40×10^{9}	1.0	6259.0
	$N+OH \rightarrow NO+H$	4.10×10^{13}	0.0	0.0

Table 7 Continued

Authors	Reaction	A (cm^3/mol-s)	b	E_A (cal/mol)
Glarborg et al.	$N+NO \rightarrow N_2+O$	9.40×10^{12}	0.14	0.0
	$N+O_2 \rightarrow NO+O$	6.40×10^{9}	1.0	6280.0
	$N+OH \rightarrow NO+H$	3.80×10^{13}	0.0	0.0

[1] From Raine et al. [51] which includes reverse reaction data from Hanson and Salimian

The rate data comparison shows that very different predictions of NO_x emissions are produced between certain sets, but all sets follow the same relative trend from run to run. The discrepancy between datasets is observed well in the comparison of the k_1 values from each set when plotted over the appropriate range of burned gas temperatures, as shown in Figure 21. Since k_1 is most influential on the mechanism, NO_x predictions trend in the same way for a given TER (or temperature).

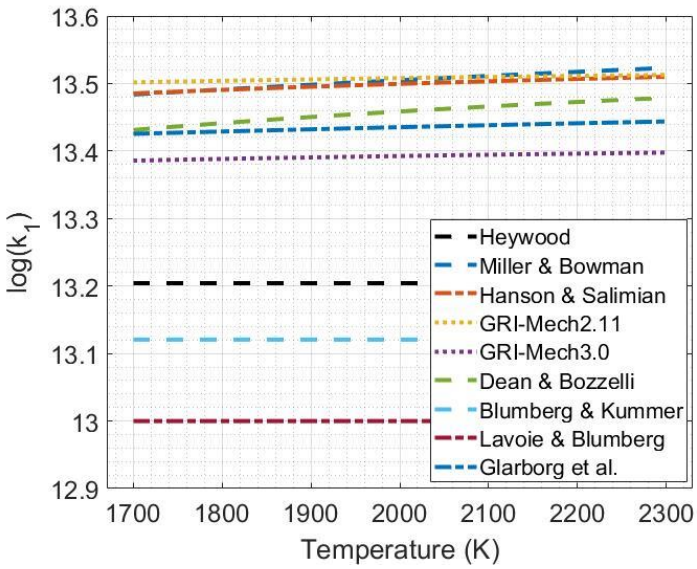

Figure 21: log(k_1) for various extended Zeldovich rate data versus temperature

Figure 22 shows the mean absolute errors (MAE) for the 9 sets of rate data. Three MAEs are reported for each set; one for all 10 nominal cases, one for the two richest cases, and one for the eight leanest cases. It was necessary to investigate these independently since the extreme errors in rich cases can be masked in the total MAE by the smaller errors in the eight lean cases. The MAEs for the eight leanest cases, also the more representative cases, are also shown separately in Figure 23.

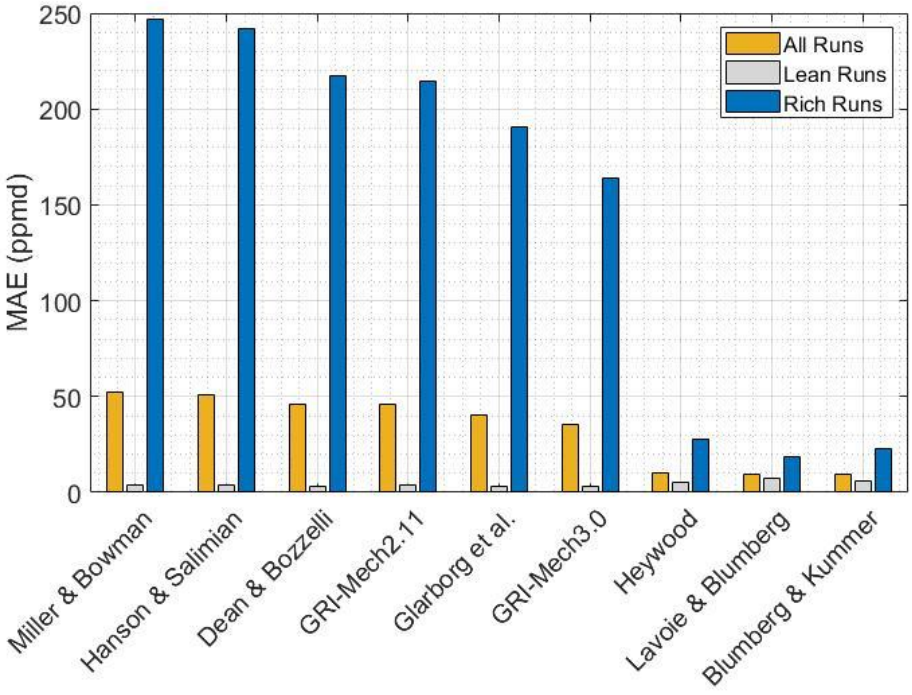

Figure 22: MAEs for each set of extended Zeldovich rate data.

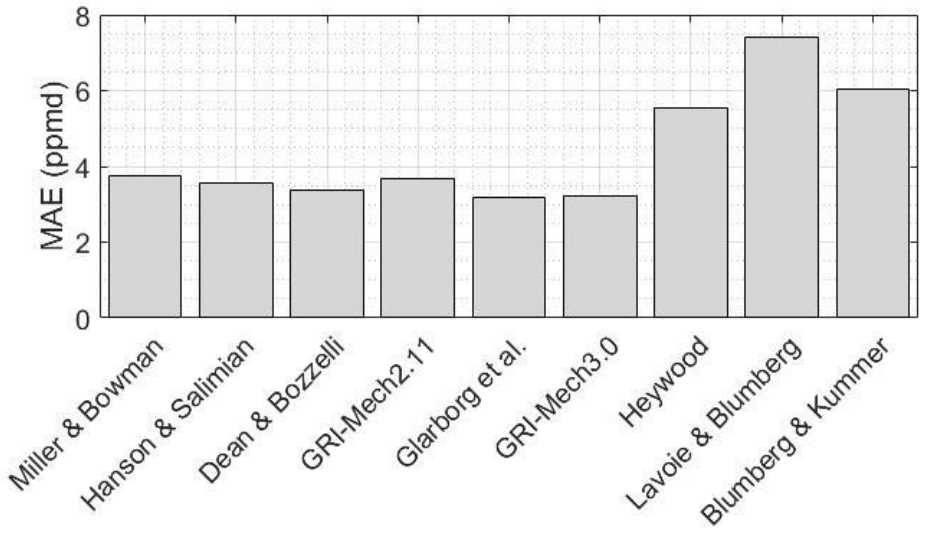

Figure 23: MAEs for lean runs using 9 set of rate data.

Error results indicate that rate data from GRI-Mech3.0 and Glarborg et al. lead to the lowest MAEs for the lean cases, but have among the worst overall MAEs due to their large over predictions at rich conditions. However, rate data from Blumberg and Kummer, Lavoie and Blumberg, and Heywood have the worst lean MAEs due to their under predictions, but have the best overall MAEs since the richest cases follow experimental values much more closely.

The excellent lean-case agreement with rate data such as from GRI-Mech3.0 could indicate that NO_x formation for the real engine is heavily dictated by the activity of thermal NO. Though the model is a 0D open chamber representation of the engine, the trends in model temperatures clearly allow for decent predictions of NO_x formation when considering only the extended Zeldovich mechanism. That said, as conditions become richer, the performance of the GRI rate data worsens. This is mostly attributed to the inability of the model to account for the stratification in the real engine which

helps to keep NO_x formation low. Since global temperatures in the model are likely higher overall than the real engine, this could result in an over prediction of NO_x like that observed here. The functionality for the k_1 values from Lavoie and Blumberg, Blumberg and Kummer, and Heywood help to keep NO_x formation lower at the richer conditions, making for a better overall prediction, but result in under predictions for the eight leanest cases more typical of the engine's operation.

Overall, this study shows that it is possible that a set of extended Zeldovich rate data could be selected to achieve relatively accurate NO_x predictions from the engine for typical conditions. That said, it is known from literature that extremely lean conditions lead to nontrivial contributions of NO_x from other pathways. This fact may lead to errors if thermal NO is considered alone and warranted further investigation into the possible contributions of other NO pathways, as predicted by the model.

4.2. Full Mechanism Implementation

To investigate the importance of other NO pathways at engine conditions, the full GRI 3.0 mechanism was used in GT-Power's burned zone kinetics. This way, the equilibrium reactions for combustion are overridden and product concentrations are calculated with the mechanism at the burned zone gas conditions. The mechanism does not affect the burn rate or any other combustion parameters.

GRI-Mech3.0, with 325 reactions and 53 species, was chosen for several reasons. Most importantly, the mechanism includes reactions for all four primary NO pathways. Since the mechanism's thermal NO sub-mechanism resulted in the lowest MAE for

normal conditions, it was desirable to see how use of the entire mechanism would change predictions. Additionally, the GRI mechanism includes formation and destruction reactions for NO_2 which was also briefly analyzed, but not scrutinized, since total NO_x predictions were of most concern. Lastly, the moderate size of the mechanism allowed for reasonable computation times of the simulation. Figure 24 shows NO_x predictions for the 10 nominal cases.

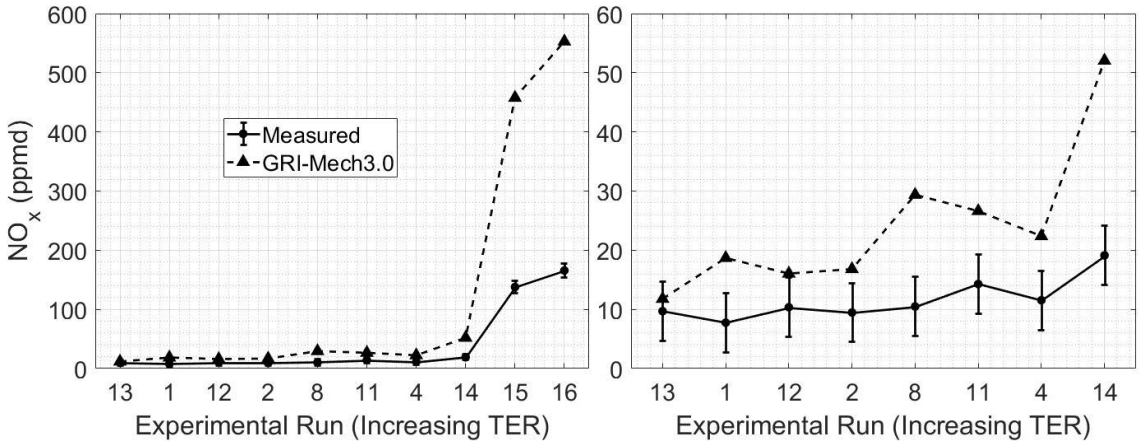

Figure 24: (Left) Experimental NO_x and predicted NO_x, versus experimental run, using full GRI-Mech3.0. (Right) 8 leanest cases.

When using the GRI mechanism, lean cases were moderately over predicted and the richest cases experienced severe over predictions. Once again, these errors are primarily attributed to the limitations in capturing the combustion in a prechambered engine. However, with all relevant NO pathways included in the predictions, further assessment could be made about the importance of non-thermal reactions at model conditions. NO_2 predictions gave insight to additional limitations of the model and, though not of major importance to the main work, are discussed in Appendix A.

4.2.1. NO Pathway Contributions

Contributions from the different NO pathways were investigated to understand how the reaction kinetics were behaving in response to the wide TER range for the 10 nominal runs. Contributions were identified through deactivation of each NO mechanism within the GRI mechanism. Calculating the difference in NO_x between the full GRI mechanism and the modified mechanism then provided the contribution from the respective pathway. Figure 25 shows the pathway contributions across the 10 nominal runs in terms of a percentage of the total NO_x level predicted with the full mechanism.

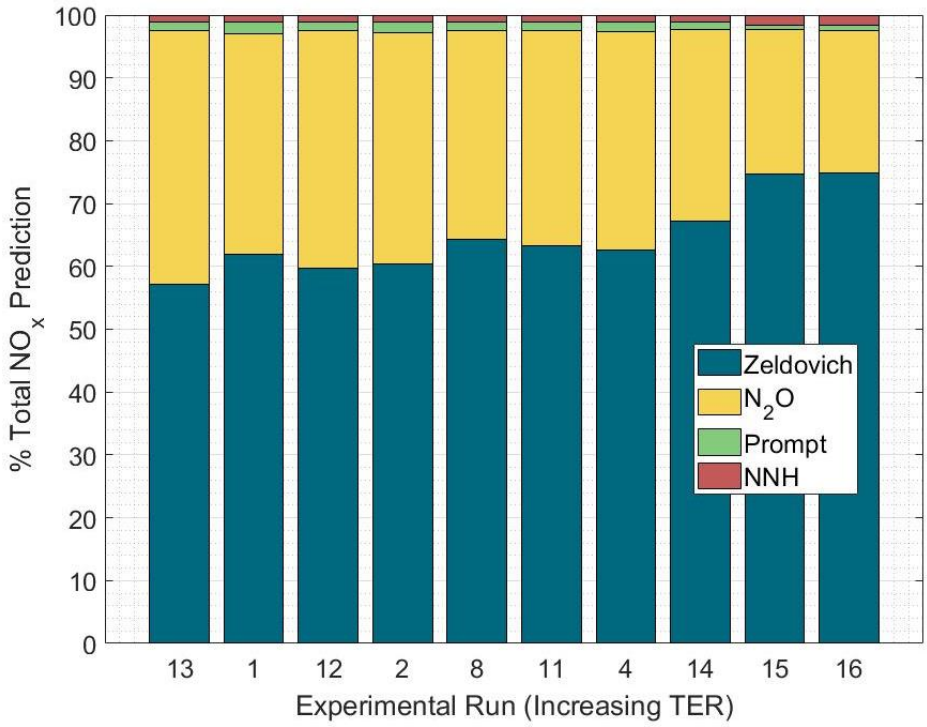

Figure 25: Stacked contributions of the 4 primary NO mechanisms to total NO_x prediction for each nominal run using GRI-Mech3.0.

The pathway contributions indicate several salient points. First, it is seen that the nitrous oxide mechanism contributes nontrivially across the TER range and even accounts for as much as >35% of total NO_x for the leanest condition. This contribution decreases as TER richens and the thermal NO contribution increases. Additionally, it is seen that, for all cases, the prompt and NNH mechanisms contribute negligibly to total NO_x, each contributing <5% for all runs. It was observed that the thermal NO contributions were slightly larger than those obtained when using the GRI-Mech3.0 extended Zeldovich rate data with equilibrium combustion in section 4.1. This is likely explained by a slightly higher burned gas temperature reached with the GRI mechanism, as well as differences in the burned zone concentrations used for thermal NO production.

4.2.1.1. Pathway Reaction Analysis

In addition to overall pathway contributions, it was desirable to know which reactions were driving NO formation across all conditions, particularly for the N_2O mechanism, in order to draw comparisons to more detailed models from literature. GT-Power does not currently include a way to view individual reaction rates of production in the burned zone gas; therefore, a separate approach was taken which utilized CHEMKIN's spark-ignited engine module to recreate the cylinder-1 pressure and burned gas temperature profiles as calculated by GT-Power.

Pressure and burned temperature profiles for Runs 13 and 15 (lean and rich runs) were matched as closely in CHEMKIN with the use of Wiebe function burn rate parameters. Perfect matches were difficult to obtain due to other tuning multipliers

available in GT-Power which affect the burn rate and heat transfer characteristics. Nonetheless, acceptable matches were obtained which closely mimicked the GT-Power results and produced similar in-cylinder NO_x profiles as well. Figure 26, Figure 27, and Figure 28 show how these profiles match for Run-13. Table 8 summarizes the key pressure and temperature values for both simulations to highlight their minor differences. Profiles for Run-15 are provided in Appendix B.

Table 8: GT-Power and CHEMKIN pressure and temperature parameters.

	RUN-13		**RUN-15**	
Software	CHEMKIN	GT-P	CHEMKIN	GT-P
Peak Pressure (bar)	43.41	43.48	43.55	43.87
LoPP (°aTDC)	20.2	22.5	16.0	18.6
Peak Temperature (K)	1930	1905	2142	2123

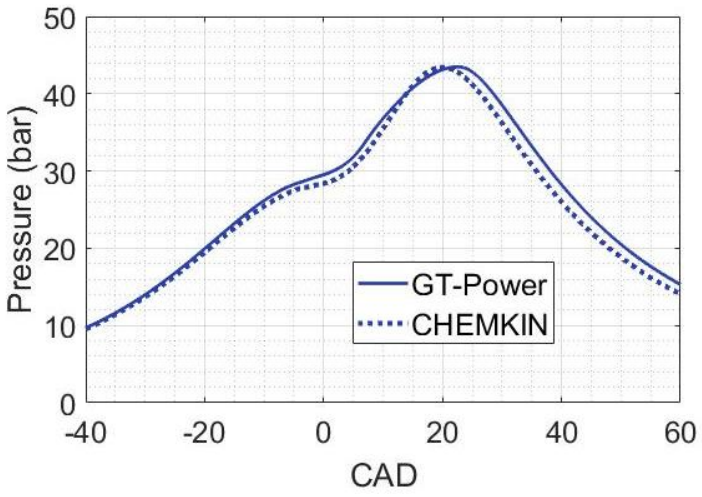

Figure 26: Simulated in-cylinder pressure using GT-Power and reproduced pressure using CHEMKIN for Run-13.

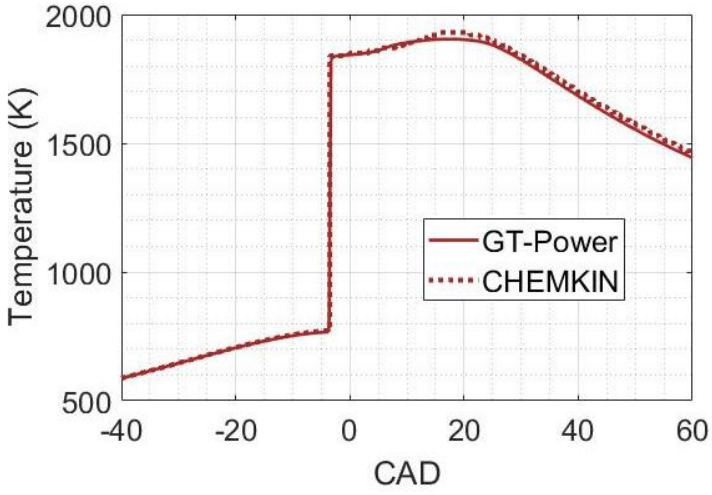

Figure 27: Simulated burned zone gas temperature using GT-Power and reproduced burned temperature using CHEMKIN for Run-13.

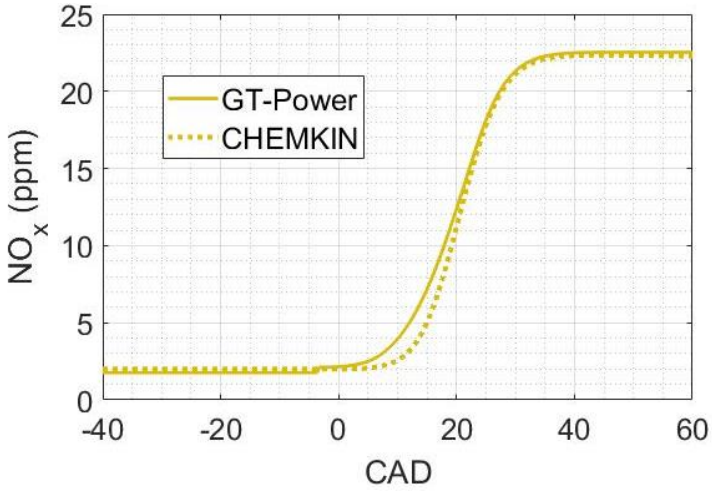

Figure 28: Simulated in-cylinder NO_x using GT-Power and reproduced in-cylinder NO_x using CHEMKIN for Run-13.

From this point, CHEMKIN's reaction path analyzer was used to investigate the prominent NO reactions for the two conditions, as inspired by the approach of Pundle [58]. Figure 29 shows the paths to NO in the burned zone for Run-13 at the peak of NO production. Arrow thickness is proportional to the absolute rate of production (ROP).

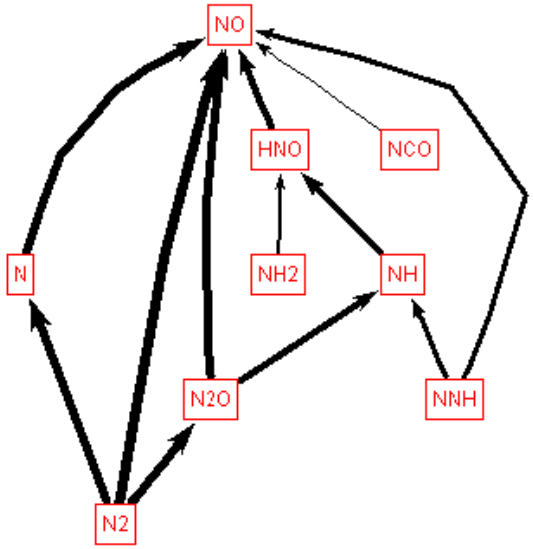

Figure 29: Pathways to NO for the leanest condition, Run-13.

Figure 30 shows the reactions involving NO and their absolute ROPs. The two highest producing reactions are the first two reactions of the extended Zeldovich mechanism. The third highest producing reaction comes from the N_2O mechanism and has just slightly lower ROP than those of the first two thermal NO reactions. These results are consistent with the overall contributions explored earlier. By far, these top three reactions produce the most NO, with the fourth highest producing reaction (also from the N_2O mechanism) having an ROP less than one tenth that of the third reaction. ROPs for reactions involving N_2O are shown in Figure 31 to confirm that the N_2O used for NO production primarily originates from the three-body reaction with N_2 and O.

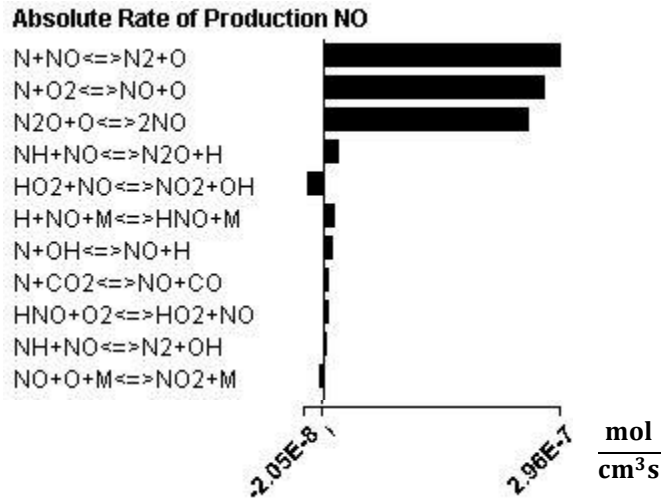

Figure 30: ROPs of the most prominent NO reactions in leanest condition, Run-13.

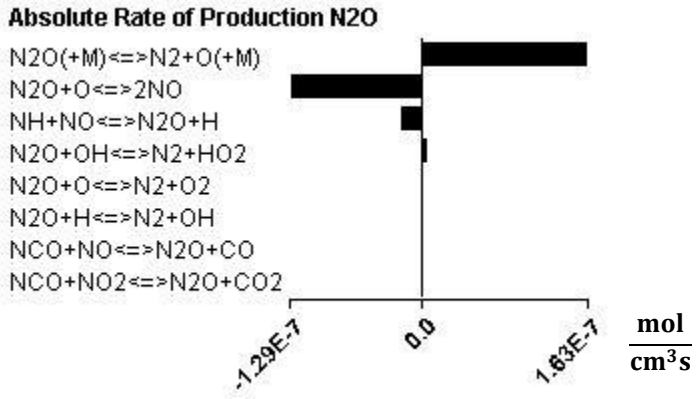

Figure 31: ROPs of the most prominent N_2O reactions in leanest condition, Run-13.

The NO chemical paths for Run-15 are basically identical to those of Run-13, with different ROPs and reaction rankings. Figure 32 shows the reactions involving NO and their absolute ROPs for Run-15. The three highest producing reactions are identical to those for Run-13; however, a dramatic relative decrease is observed in the ROP of the third reaction. Here, the N_2O reaction to NO has an ROP less than half of either of the extended Zeldovich reactions. This also aligns with the overall contribution results from

GT-Power discussed earlier. Figure 31 shows that, like the lean condition, the N_2O originates from the three-body reaction with N_2 and O.

The reaction $N_2O+H \leftrightarrow NH+NO$, from the N_2O mechanism, appears to also participate nontrivially in the formation of NO for both conditions, but more so for the richer Run-15. This is also observed in Figure 33 which indicates that a fair amount of N_2O is used up by the reaction. In the case of Run-13, this reaction even out produces the third reaction of the extended Zeldovich mechanism ($N+OH \leftrightarrow NO+H$).

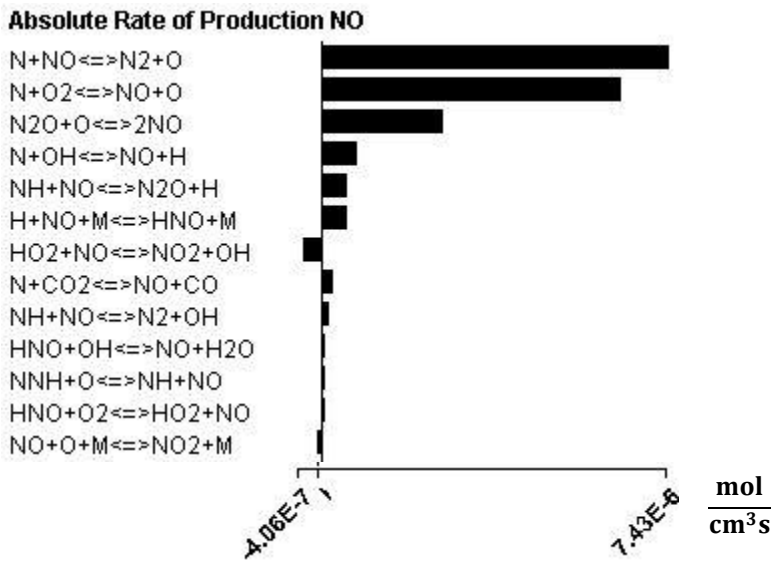

Figure 32: ROPs of the most prominent NO reactions in rich condition, Run-15.

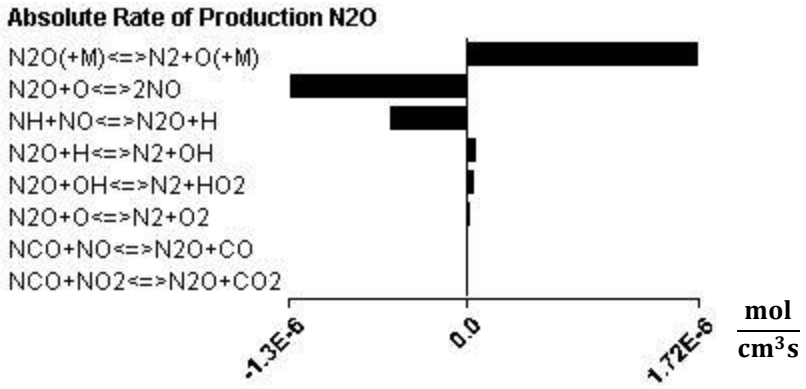

Figure 33: ROPs of the most prominent N_2O reactions in rich condition, Run-15.

4.3. Reduced NO_x Mechanism

Results from the mechanism contribution and reaction pathway analysis indicate that the extended Zeldovich mechanism and N_2O mechanism account for most of the NO produced in the model for the leanest and richest conditions simulated. This complements the findings of other authors in literature, some of whom more accurately modeled the in-cylinder combustion process and emissions formation of similar engines. Therefore, these results confirm that the 0D/1D, two-zone model, while limited, is able to retain representative behavior of the real engine and more advanced models.

Additionally, from the pathway analysis, it is seen that three notable reactions appear to facilitate the formation of most N_2O-formed NO in the model which also agrees well with literature findings. This indicates that simulating NO_x production in the GT-Power model could be achieved with a simple set of the important reactions noted from the CHEMKIN pathway analysis at the engine conditions. The reactions identified for primary NO production are summarized in Table 9.

Table 9: Primary reactions identified for use in NO_x mechanism.

Extended Zeldovich Mechanism	**NOTE**
$N + NO \leftrightarrow N_2 + O$	Forms the most NO for leanest and richest cases.
$N + O_2 \leftrightarrow NO + O$	Forms second-most NO for leanest and richest cases.
$N + OH \leftrightarrow NO + H$	Mostly important for NO formation at richest cases.
N_2O Mechanism	**NOTE**
$N_2O(+M) \leftrightarrow N_2 + O(+M)$	Forms the most N_2O for leanest and richest cases.
$N_2O + O \leftrightarrow 2NO$	Forms third-most NO for leanest and richest cases.
$NH + NO \leftrightarrow N_2O + H$	Small but nontrivial NO production at both cases, more important for richest.

The advantage of using the simplified set of reactions in Table 9 is that they can be used with GT-Power's default equilibrium combustion without the need for oxidation reactions in burned zone kinetics. In this case, concentrations of N, N_2, O, O_2, H, and OH are calculated through equilibrium. All other species are then determined through kinetics. The lack of full oxidation kinetics reduces simulation run times from ~65 minutes (with full GRI mechanism) to ~5 minutes per operating condition.

Including the last reaction, which produces NH, necessitates the use of additional reactions in order to be used by the software. In work discussed earlier [34] [35] [58] the NH produced from this reaction is assumed to react completely to NO, which is acceptable for lean, premixed combustion. Here, two additional reactions are included in the reduced NO_x mechanism to promote the conversion of NH to NO; these are

$$NH + O_2 \leftrightarrow NO + OH \quad (32)$$

$$NH + O \leftrightarrow NO + H \quad (33)$$

These reactions were chosen due to their forward procession to NO observed in CHEMKIN, as well as their usage of only NH, NO, and species included in equilibrium. There was also a prominent pathway from NH to NO which included HNO, but this pathway relied on other intermediate species. The reactions chosen to represent the N_2O mechanism account for the majority of its NO contribution for the modeled conditions.

Two reduced NO_x mechanisms were developed using the reactions identified in the previous section. Each mechanism uses the N_2O rate data from the GRI mechanism, but use different sets of extended Zeldovich rate data. One mechanism, labeled *B&K/N_2O*, uses the extended Zeldovich rate data cited by Blumberg and Kummer [50]. The other mechanism, *L&B/N_2O*, uses extended Zeldovich rate data cited by Lavoie and Blumberg [52]. These sets of thermal rate data were chosen because of their best overall MAEs, but clear under predictions in the leaner cases when used alone. Results from using the two improved mechanisms are shown in Figure 34.

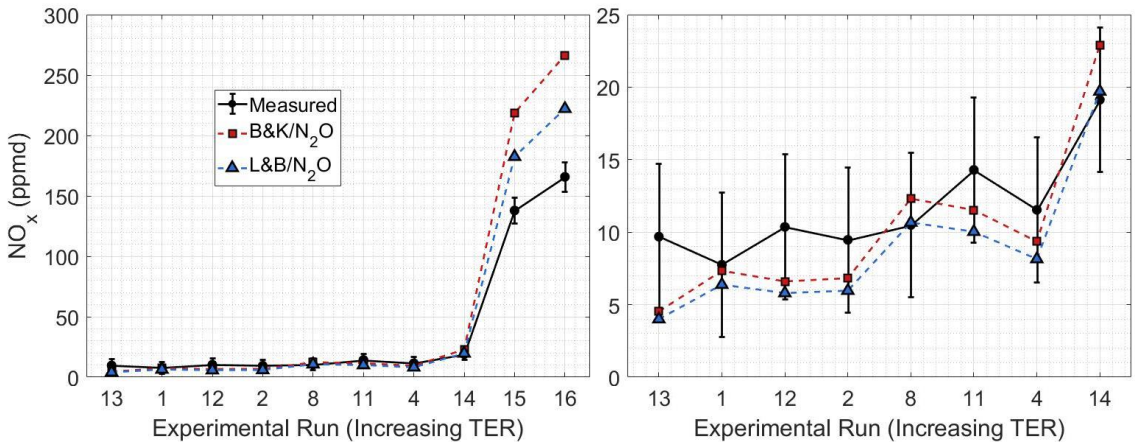

Figure 34: (Left) Measured NO_x and simulated NO_x when using two reduced NO_x mechanisms with different thermal rate data. (Right) 8 leanest cases.

Overall, the two mechanisms lead to improved results, particularly for the lean cases. As seen in Figure 35, both lean MAEs decrease by over 50% when the N_2O mechanism is included. Each mechanism also achieves a slightly smaller error for the eight leanest cases than that obtained with the GRI thermal mechanism alone.

These mechanisms clearly satisfy the prediction needs for the model. A noticeable over prediction is still observed in the two richest conditions, but the agreement for these runs is still greatly improved. Further, it is possible that a single mechanism, as proposed here, may not be able to produce adequate NO_x predictions across a large TER range unless additional tuning is utilized. This may simply be a result of the barriers inherent to the 0D, two-zone modeling approach used here. Nonetheless, conditions like Run-15 and 16 are uncommon to this engine, making their accuracy less important for most studies.

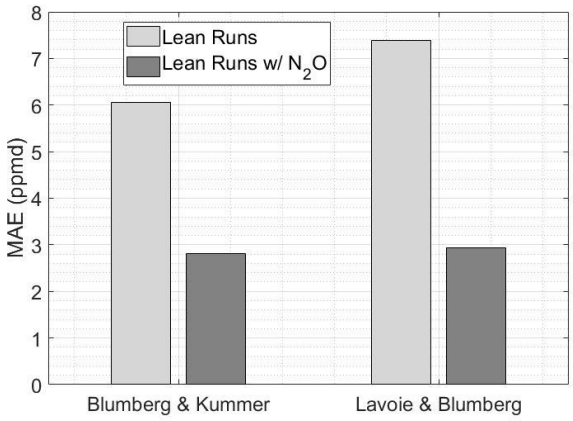

Figure 35: MAEs of two best extended Zeldovich rate datasets with and without the inclusion of the N_2O mechanism.

Figure 36 compares the NO_x predictions obtained with GRI thermal NO and the best reduced mechanism using rate data from Blumberg and Kummer. As indicated earlier, improvements with the reduced mechanism are minor, but undoubtedly show slightly better agreement at the leanest and richest ends where the GRI thermal mechanism alone tends to under predict and over predict, respectively.

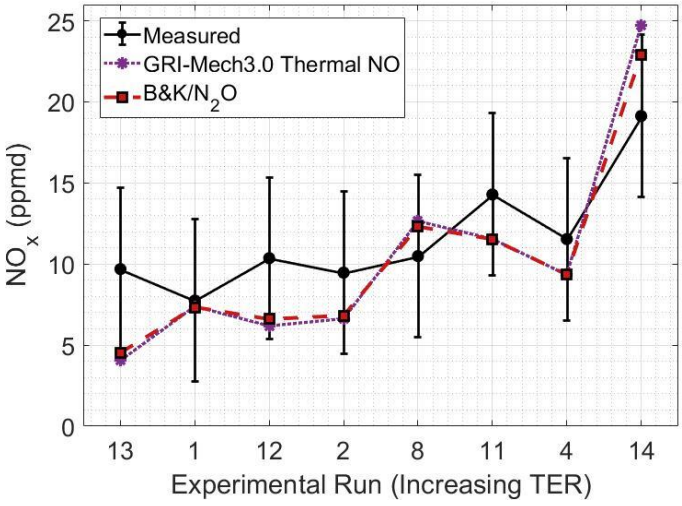

Figure 36: Comparison of reduced mechanism and GRI-Mech3.0 thermal NO.

4.4. Full Mechanism Reduction

An attempt was made at creating reduced combustion mechanisms using the reproduced CHEMKIN cycles and the software's mechanism reduction tool. With a reduced mechanism, burned zone kinetics in GT-Power could still include other reactions which affect NO_x formation, without including too many unimportant species or steps. Thus, simulation times could be reduced while still retaining NO_x predictions similar to the full mechanism. Use of a reduced combustion mechanism was explored but abandoned here due to several limitations. Appendix C discusses that approach.

4.5. Discussion of Further Tuning

The reduced NO_x mechanism approach discussed in the previous section allows for reasonably accurate predictions of NO_x in an acceptable amount of time. That said, the contributions of the thermal and N_2O pathways are dictated solely by the rate coefficients which resulted in the best overall fit. This means that the model may not entirely represent the contributions of the various pathways in an accurate manner. This is important to consider when engine-specific changes are made which could affect the contributions of these pathways, affecting overall predictions.

To overcome these limitations, a crude tuning method can be employed to adjust the mechanism contributions, if necessary. Such a method could include tuning factors (α_{ZELD}, α_{N_2O}**)** multiplied to the reaction rate coefficients of the two most important thermal and N_2O pathway reactions, as show in Table 10. Multipliers could be

determined by minimization of error or from knowledge of the pathway contributions found with a more accurate engine model.

Table 10: Tuning method for thermal and N_2O NO_x formation

Reaction	Reaction Rate Coefficient	Rate Data
$NO + N \rightleftarrows N_2 + O$	$k = \boldsymbol{\alpha_{ZELD}} * 1.32e13$	Blumberg & Kummer
$N_2O + O \leftrightarrow 2NO$	$k_1 = \boldsymbol{\alpha_{N_2O}} * 2.9e13 * \exp\left(\frac{-23150}{R\,T_b}\right)$	GRI-Mech3.0

A tuning approach was briefly explored here which makes an attempt at adding additional consideration for the real engine processes. This approach attempts to quantify the contributions of PCC and MCC-formed NO separately by recognizing the stratification experienced in a prechambered engine. As depicted in Figure 37, it is assumed that a fraction of total NO_x can be attributed to PCC gases ($\boldsymbol{x_{NOx,PCC}}$), and a fraction of total NO_x can be attributed to MCC gases ($\boldsymbol{x_{NOx,MCC}}$).

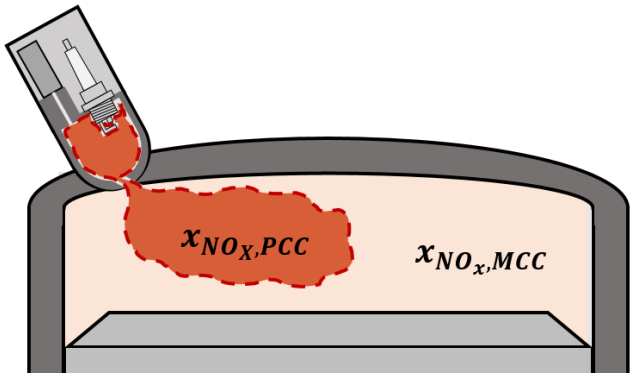

Figure 37: NO_x fractions assumed from stratification.

It is known that the PCC contributes most of the NO_x at lean engine operating conditions. Further, since the PCC operates at near-stoichiometric equivalence ratios, the combustion of its gases likely produce NO primarily through the thermal pathway. Additionally, the MCC operates well below stoichiometric levels at the lean limit, meaning that combustion of its gases may form non-trivial NO through the N_2O pathway. Thus, it could be said that there is some lower bound for the amount of thermal NO formed in the engine at the leanest conditions; this bound being nearly equal to the NO formed from the stoichiometric PCC.

This methodology led to an attempt at tuning the reduced mechanism in accordance with estimates for PCC NO_x contributions found in literature. Here, the multipliers were adjusted until 70% of total NO_x was formed through the extended Zeldovich mechanism and 30% was formed through the N_2O mechanism for the leanest condition, Run-13. Results from this tuning are show in Figure 38. Contributions from the full GRI mechanism, the *B&K/N_2O* reduced mechanism, and the PCC-tuned reduced mechanism are shown in Figure 39.

Tuning to a PCC contribution does not improve predictions from the reduced mechanism, but the addition of the N_2O mechanism still allows for improvements over the GRI thermal mechanism alone. Thus, the un-tuned *B&K/N_2O* mechanism is still identified as the best mechanism for this modeling; however, the tuning process may be useful for another engine.

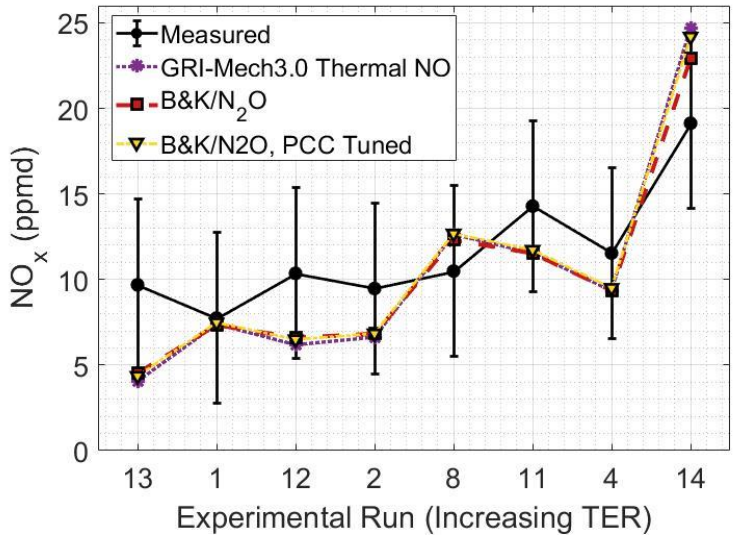

Figure 38: NO_x predictions for GRI thermal NO alone, B&K/N_2O, and tuned B&K/N_2O.

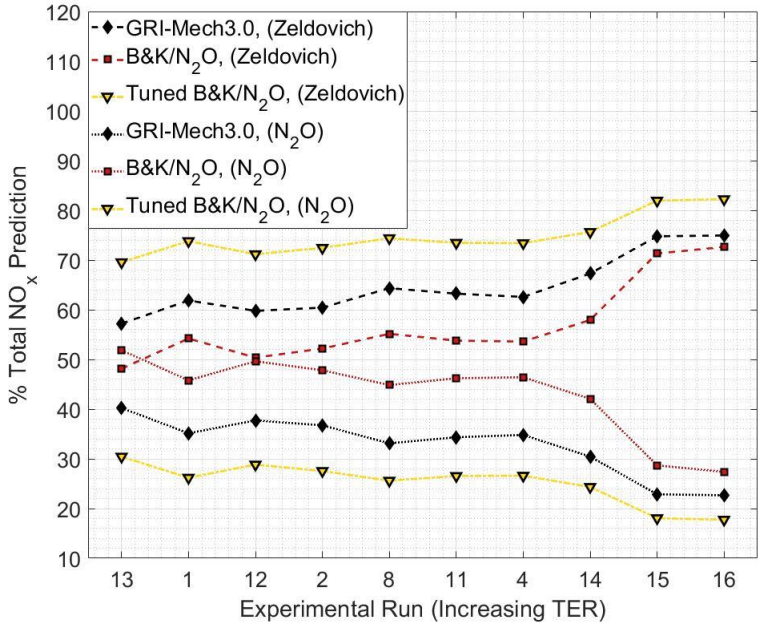

Figure 39: Zeldovich and N_2O contributions to total NO_x for full GRI-Mech3.0, B&K/N_2O, and tuned B&K/N_2O.

5. RESULTS: NO_X PREDICTION PERFORMANCE

5.1. Predictions for Various Spark Timing

The unmodified, *B&K/N_2O* mechanism discussed in the previous section is assessed further in this section with the seven additional experimental runs not used for tuning. These runs also sit well within the normal operating range of the engine, but differ in spark timing from the nominal runs used for tuning. Since NO_x formation is heavily affected by spark timing, it was important to see how the method chosen would perform for these cases.

NO_x predictions for the seven additional runs are shown in Figure 40 along with measured NO_x values. The results show good agreement with experimental values, lying acceptably within the measurement accuracy. This shows that the model and NO_x mechanism work well even for changes in spark timing.

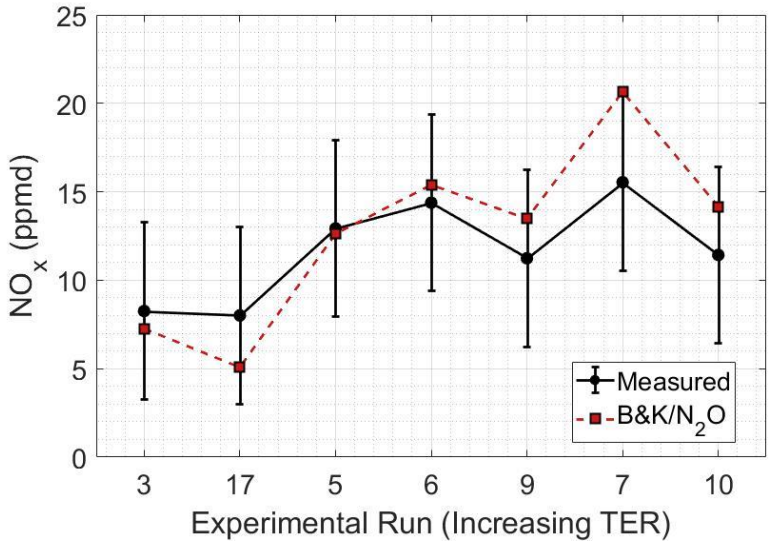

Figure 40: NO_x predictions for 7 additional runs with varying spark timing.

For a more comprehensive look, NO_x predictions for all characteristic runs are observed in Figure 41. Here it is observed that nearly all predictions fall well within the measurement accuracy, resulting in a MAE of 2.52 ppmd.

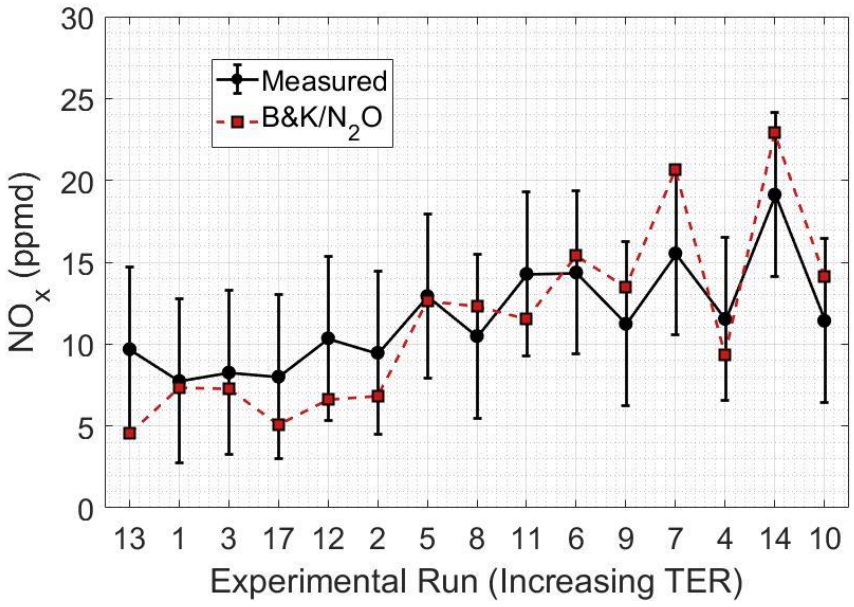

Figure 41: NO_x predictions for all lean runs when using chosen NO_x mechanism.

Three pairs of runs were observed further to more fully understand the effect that spark timing changes have on reaction kinetics in the model. The runs compared are 17 and 12, 7 and 4, and 14 and 10; they are summarized in Table 11. As seen there, each respective pair of points has nearly the same TER and torque, but differing spark timings. Thus, changes in NO_x between the respective pairs should be largely driven by the effect of spark timing changes.

Table 11: Summarization of runs compared for spark timing change

Run	TER	IT (°bTDC)	Torque (%)
17	~0.401	2	84
12		3.5	91
7	~0.410	5	90
4		3.5	91
14	~0.421	3.5	90
10		2.5	90

The NO_x values for the 3 pairs of runs compared, as well as the percentage of thermal NO contribution to the total predictions are shown in Figure 42, Figure 43, and Figure 44. It is seen that the contribution of thermal NO increases for all TER levels when spark timing is more advanced.

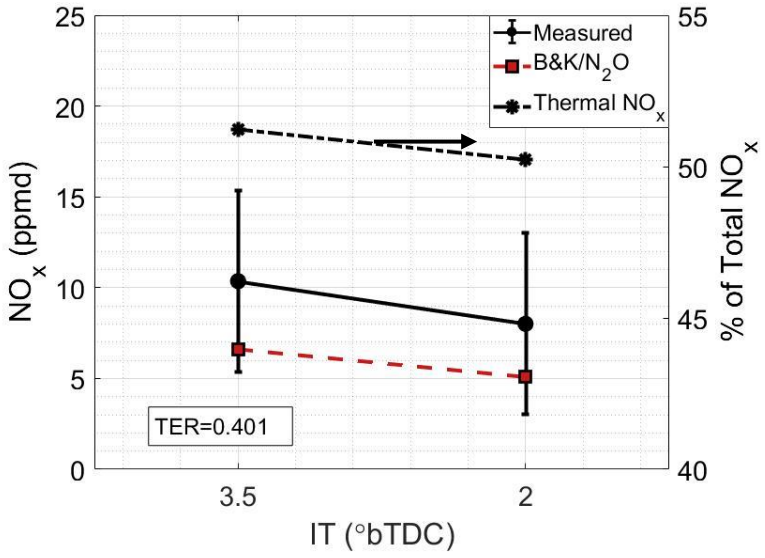

Figure 42: NO_x predictions and thermal NO contribution (Runs 12 and 17).

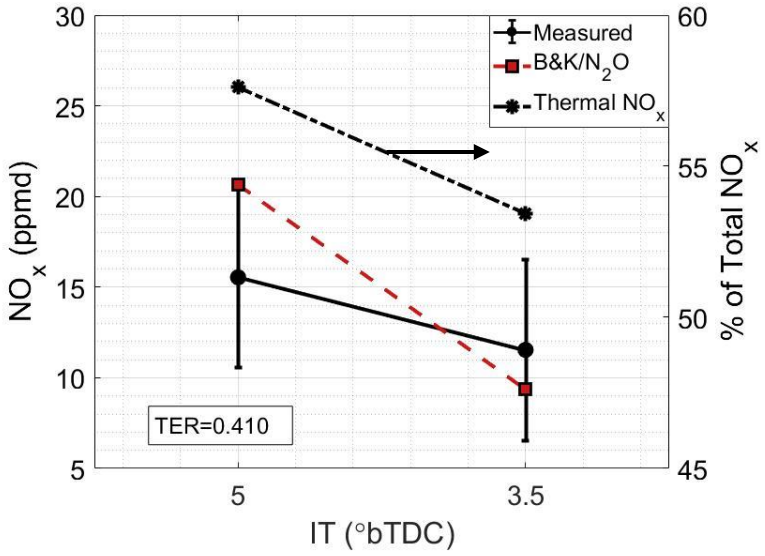

Figure 43: NO_x predictions and thermal NO contribution (Runs 7 and 4).

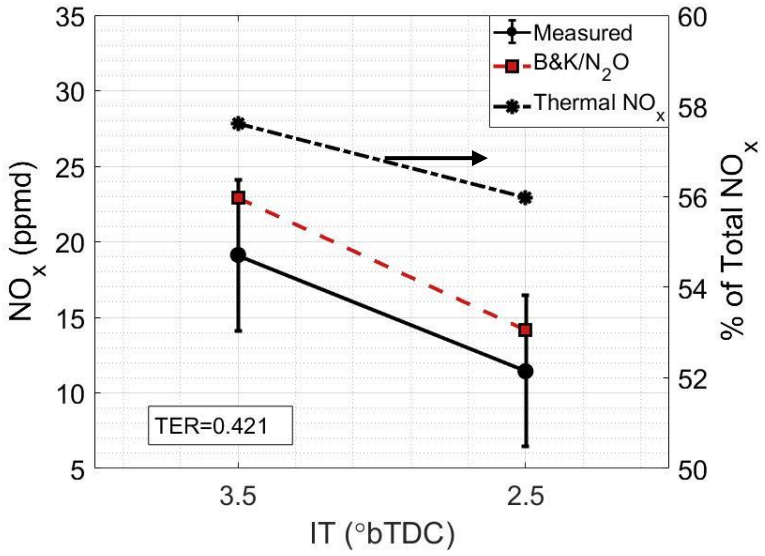

Figure 44: NO_x predictions and thermal NO contribution (Runs 14 and 10).

6. RESULTS: FUEL COMPOSITION SWEEP

Lastly, the engine model was assessed for its ability to capture the trends that would be expected for changing fuel composition. This was performed by utilizing the same simulations investigated earlier and changing the amount of fuel ethane and propane in the simulated fuel. Final tuning of the model for variable fuel composition effects was not in the main scope of work, thus, this step was intended to preliminarily judge the model. Since no variable fuel composition data was taken from the engine of interest, trends are qualitatively compared with expectations.

6.1. Changes in Ethane

Fuel ethane concentration was swept across 3 points to observe the effect on various parameters. The base fuel composition used is simply the recorded composition at time of experiment for the respective run. Then, representative high and low ethane points are provided to the model to compare against the base composition results. High and low mole fractions of ethane were prescribed based on the accuracy of the LFS equation fit supplied to the model in previous work. [28]

Table 12: Test space construction for fuel sweep points.

Component mole fraction	C2 Low	Base	C2 High
C1	Balance	Composition of respective run	Balance
C2	0.05		0.08
C3	Same as base composition		Same as base composition
C4			
C5			
CO_2			
N_2			

The parameters investigated include peak pressure (PP), location of peak pressure (LoPP), peak temperature (PT), and exhaust NO_x. Results for these parameters when observing Run-13, the leanest case, are shown in Figure 45. Results for Run-14, the richest normal operating point, are shown in Figure 46.

Results from the two runs clearly show that the model is affected by the changes in fuel composition, and parameters change in the ways that are expected. Namely, as the fuel becomes more reactive with additional ethane, the LoPP shifts earlier and results in increased peak pressures and temperatures. The resulting effect is that the amount of engine-out NO_x increases with additional ethane.

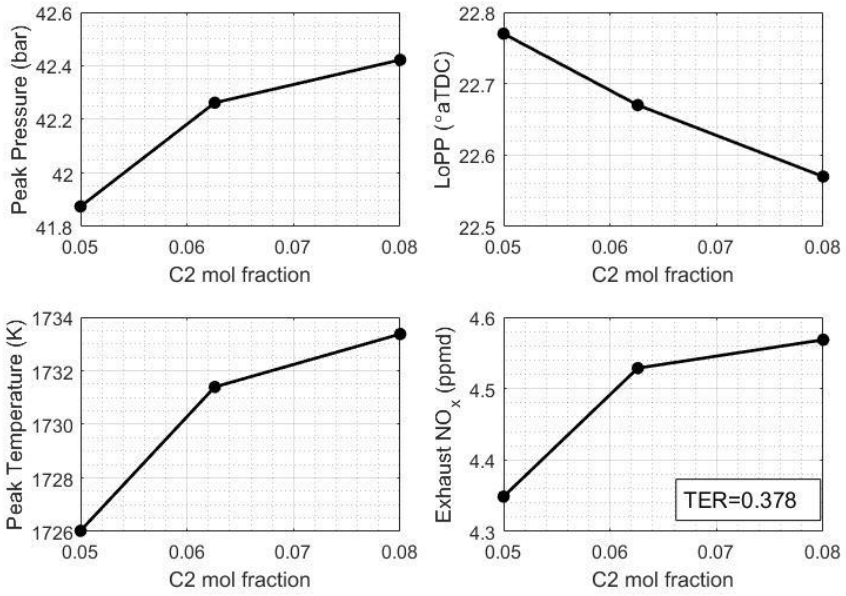

Figure 45: PP, LoPP, PT, and NO_x versus C2 mol fraction (Run-13).

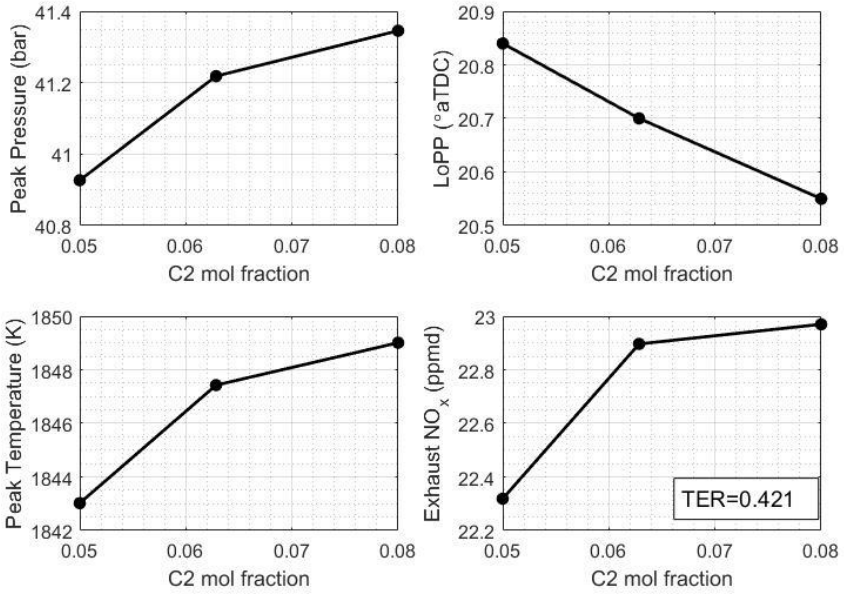

Figure 46: PP, LoPP, PT, and NO_x versus C2 mol fraction (Run-14).

6.2. Changes in Propane

The same sweep methodology used for propane mole fraction in the fuel. The corresponding high and low values tried were, again, prescribed based on the accuracy of the LFS model implemented in GT-Power. Thus, changes were small, but allowed for a qualitative assessment of the model's capabilities in capturing propane variation. Results for the parameter changes in Run-13 and Run-14 are shown in Figure 47 and Figure 48, respectively. Once again, these results show that the model is appropriately reacting to changes in fuel composition as all parameters shift in the ways that would be expected.

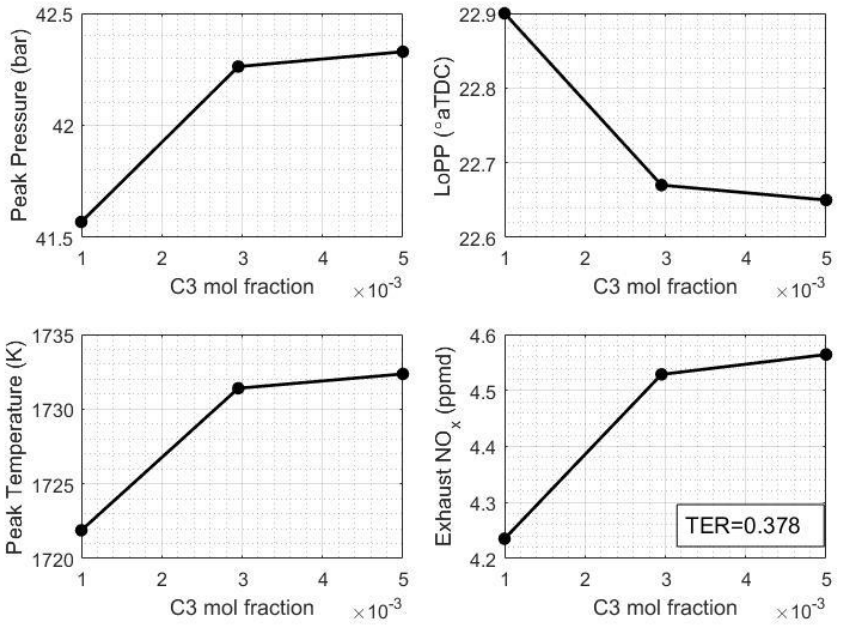

Figure 47: PP, LoPP, PT, and NO_x versus C3 mol fraction (Run-13).

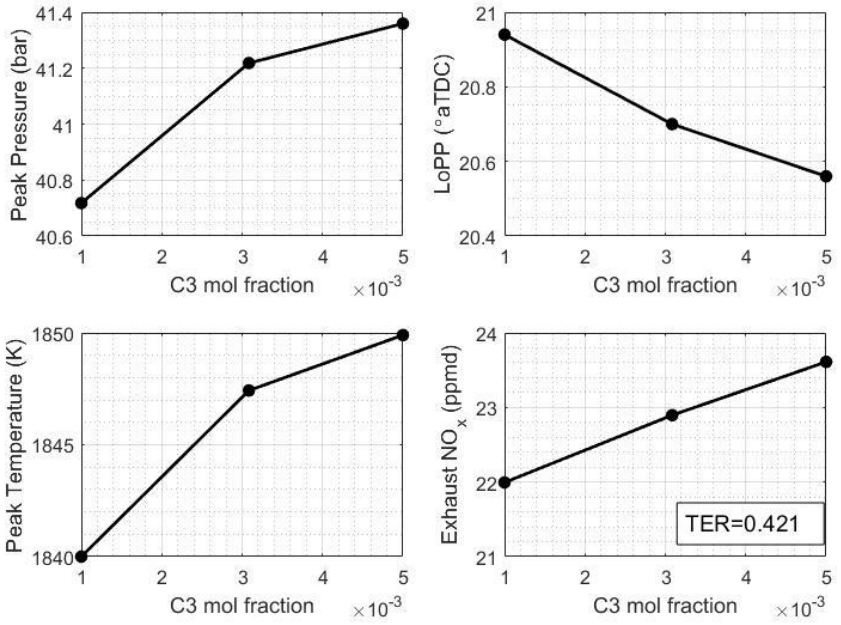

Figure 48: PP, LoPP, PT, and NO_x versus C3 mol fraction (Run-14).

7. FUTURE CONSIDERATIONS

Though this work provides a good foundation on which to base further investigations of NO_x formation with this engine model and others like it, several actions may be considered for future work. Suggestions for improvement are as follows:

1. First and foremost, the NO_x prediction method proposed should be tried in models of other, similar engines to judge robustness and possibly improve on the NO_x mechanism. This would also be useful to help assess the selection of thermal rate data that should be used for lean-burn engines. It would be particularly useful to try the proposed method for an OCC, natural gas engine with similar operating characteristics.

2. The low NO_x levels, along with relatively large measurement uncertainty at normal engine operation, made for difficult assessment and tuning of the NO_x predictions. It is possible that future work can use the method proposed here against experimental data with less uncertainty or more overall engine-out NO_x. In this way, better assessment of the NO_x prediction method can be made.

3. The fuel composition sweep explored here was limited in variation and showed small changes in simulated engine operation. To improve on this, it is suggested that a new LFS correlation be made which has sufficient accuracy for a wide range of gas compositions. Further, future work may consider the effect that fuel composition has on engine operation by way of changing ignition delay as well.

4. If high levels of NO_x accuracy are desired, the development of a model including detailed prechamber characteristics is recommended. This can be attempted with GT-Power, CFD, or by developing a model from a first-principles approach.

8. CONCLUSION

In this work, NO_x emissions prediction capabilities were added to the full-scale engine simulation of a Cooper-Bessemer GMWH-10C. Predictions were attempted via several approaches to arrive at a method which can be easily implemented into the engine model and retains suitable accuracy for typical engine operating conditions.

Predictions were first explored with the extended Zeldovich mechanism alone. This method showed fairly good agreement for particular sets of extended Zeldovich rate data, indicating that the real engine's NO_x formation may be heavily influenced by the activity of thermal NO. However, the consideration of thermal NO alone led to slightly worse agreement for the leanest and richest conditions observed.

Additional investigation was given to the contributions of all NO formation pathways when included in the model via a full combustion mechanism. Results showed that thermal and N_2O pathways accounted for most NO formed. Further investigation using detailed reaction pathway analysis led to the development of a reduced NO_x mechanism including eight key reactions which were chosen to characterize the formation of NO_x through the extended Zeldovich mechanism and N_2O mechanism.

The reduced NO_x mechanism not only led to the best overall agreement with experimental runs used for testing, but also performed with equally suitable accuracy for additional runs which varied in spark timing. The engine model also showed acceptable results for a sweep of fuel composition. It is expected that the engine model can now be more rigorously tested against variable fuel composition emissions data.

REFERENCES

[1] U.S. Energy Information Administration, "Natural Gas Explained," December 2018. [Online]. Available: https://www.eia.gov/energyexplained/index.php?page=natural_gas_home.

[2] R. E. Braziel, The Domino Effect: How the Shale Revolution is Transforming Energy Markets, Industries and Economics, Houston: NTA Press, 2016.

[3] U.S. Energy Information Administration, "How much shale gas is produced in the United States?," 10 2018. [Online]. Available: https://www.eia.gov/tools/faqs/faq.php?id=907&t=8.

[4] U.S. Energy Information Administration, "Annual Energy Outlook 2019 with Projections to 2050," United States Energy Information Administration, 2019.

[5] G. Choquette, "Analysis and Estimation of Stoichiometric Air-Fuel Ratio and Methane Number for Natural Gas," in *Gas Machinery Conference*, Nashville, 2014.

[6] S. Turns, An Introduction to Combustion: Concepts and Applications, New York: McGraw-Hill, 2012.

[7] J. Hedrick and T. Jacobs, "A Review of Variable Natural Gas Composition, Effects, and Control Mehtods for Reliable Combustion in Lean Burn Two-Stroke Engines," Pipeline Research Council International, 2015.

[8] K. Fieseler and T. J. Jacobs, "Variable NG Composition Effects on LB 2SC Integral Engines, Phase III - Predictive Combustion Modeling," Pipeline Research Council International, 2018.

[9] U.S. Energy Information Administration, "About U.S. Natural Gas Pipelines - Transporting Natrual Gas," U.S. Energy Information Administration, 2008. [Online]. Available: https://www.eia.gov/naturalgas/archive/analysis_publications/ngpipeline/index.html.

[10] U. E. I. Administration, "Natural Gas Explained: Natural Gas Pipelines," December 2018. [Online]. Available: https://www.eia.gov/energyexplained/index.php?page=natural_gas_pipelines.

[11] Advanced Engine Technologies Corporation and et al., "Pipeline Engine Emissions Control Roadmap," Pipeline Research Council International, 2005.

[12] G. Beshouri, T. J. Jacobs and G. Choquette, "The Impact of Varying Fuel Speciation on Engines Using "Virtual Sensor" Air/Fuel Ratio Controls," in *Dessau Gas Engine Conference*, Dessau-Roßlau, 2019.

[13] U.S. Energy Information Administration, "U.S. Natural Gas Pipeline Compressor Stations Illustration," U.S. Energy Information Administration, 2008. [Online]. Available: https://www.eia.gov/naturalgas/archive/analysis_publications/ngpipeline/compressorMap.html.

[14] D. Olsen, J. Adair and B. Willson, "Precombustion Chamber Design and Performance Studies for a Large Bore Natural Gas Engine," in *ASME Internal Combustion Engine Division 2005 Spring Technical Conference*, Chicago, 2005.

[15] D. Simpson and D. Olsen, "Precombustion Chamber Design for Emissions Reduction From Large Bore NG Engines," *Journal of Engineering for Gas Turbines and Power,* vol. 132, no. 12, pp. 122802-122802-7, 2010.

[16] C. Bowman, "Kinetics of Pollutant Formation and Destruction in Combustion," *Progress in Energy and Combustion Science,* vol. 1, no. 1, pp. 33-45, 1975.

[17] J. Santner, S. Ahmed, T. Farouk and D. Dryer, "Computational Study of NOx Formation at Conditions Relevant to Gas Turbine Operation: Part 1," *Energy and Fuels,* vol. 30, pp. 6745-6755, 2016.

[18] C. A. T. Center, *Nitrogen Oxides (NOx), Why and How They Are Controlled,* U.S. Environmental Protection Agency , 1999.

[19] U. E. P. Agency, "Nitrogen Dioxide (NO2) Pollution, Basic Information about NO2," September 2016. [Online]. Available: https://www.epa.gov/no2-pollution/basic-information-about-no2#What%20is%20NO2.

[20] A. Glassman and R. Yetter, Combustion, Cambridge, MA: Academic Press, 2008.

[21] O. o. A. a. Radiation, *Nitorgen Oxides: Impacts on Public Health and the Environment,* Washington DC: U.S. Environmental Protection Agency , 1997.

[22] R. Casiday and R. Frey, "Acid Rain, Inorganic Reactions Experiment," Department of Chemistry, Washinting University, 1998. [Online]. Available: http://www.chemistry.wustl.edu/~edudev/LabTutorials/Water/FreshWater/acidrain.html.

[23] P. Nelson, "Reduction of NOx Emissions from Stationary Combustion Sources," *Transactions of the Institution of Engineers, Australia* , vol. 17, pp. 59-64, 1992.

[24] *Code of Federal Regulations, Title 40, Part 60,* 2018.

[25] T. Linker and T. Jacobs, "Variable Fuel Effects on Legacy Compressor Engines, Phase IV - Predictive NOx Modeling," Pipeline Research Council International, 2019.

[26] J. Caton, An Introduction to Thermodynamic Cycle Simulations for Internal Combustion Engines, Chichester, West Sussex: John Wiley & Sons Ltd, 2016.

[27] J. Heywood, Internal Combustion Engine Fundamentals, New York: McGraw-Hill, 1988.

[28] K. Fieseler, *Simulation Development of a Large Bore Two Stroke Integral Compressor Engine to Study Variable Natural Gas Composition Effects*, MS Thesis, Texas A&M University, 2018.

[29] Gamma Technologies, Inc., GT-SUITE Engine Performance Application Manual, Version 2017, 2016.

[30] Y. Zeldovich, P. Sadovnikov and D. Frank-Kamenetskii, *Oxidation of Nitrogen in Combustion*, Moscow-Leningrad: Academy of Sciences USSR, Institute of Chemical Physics, 1947.

[31] G. A. Lavoie, J. B. Heywood and C. J. Keck, "Experimental and Theoretical Study of Nitric Oxide Formation in Internal Combustion Engines," *Combustion Science and Technology*, vol. 1:4, pp. 313-326, 1970.

[32] S. Turns, An Introduction to Combustion: Concepts and Applications, New York: McGraw-Hill, 2012.

[33] P. Malte and D. Pratt, "The Role of Energy-Releasing Kinetics in NOx Formation: Fuel-Lean, Jet-Stirred CO-Air Combustion," *Combustion Science and Technology*, vol. 9, pp. 221-231, 1974.

[34] A. Pundle, D. Nicol, P. Malte and J. Hiltner, "Modeling the Formation of Pollutant Emissions in Large-Bore, Lean-Burn Gas Engines," in *ASME Internal Combustion Engine Division Fall Technical Conference*, 2017.

[35] I. Novosselov and P. Malte, "Development and Applications of an Eight-Step Global Mechanism for CFD and CRN Simulations of Lean-Premixed Combustors," *Journal of Engineering for Gas Turbines and Power*, vol. 130, no. 2, pp. 769-779, 2008.

[36] M. Drake and R. Blint, "Calculations of NOx Formation Pathways in Propogating Laminar, High Pressure Premixed CH4/Air Flames," *Combustion Science and Technology*, vol. 75, pp. 261-285, 1991.

[37] C. Fenimore, "Formation of Nitric Oxide in Premixed Hydrocarbon Flames," *Symposium (International) on Combustion,* vol. 13, no. 1, pp. 373-380, 1971.

[38] G. Lavoie and P. Blumberg, "Measurements of NO Emissions From a Stratified Charge Engine: Comparison of Theory and Experiment," *Combustion Science and Technology,* vol. 8, no. 1-2, pp. 25-37, 1973.

[39] G. Leonard and S. Correa, *NOx Formation in Premixed High-Pressure Lean Methane Flames,* Fossil Fuel Combustion Symposium, 1990 : presented at the Thirteenth Annual Energy-Sources Technology Conference and Exhibition, New Orleans, Louisiana, 1990.

[40] J. Bozzelli and A. Dean, "O+NNH: A Possible New Route for NOx Formation in Flames," *International Journal of Chemical Kinetics*, vol. 27, pp. 1097-1109, 1995.

[41] S. Klippenstein, L. Harding, P. Glarborg and J. Miller, "The role of NNH in NO formation and control," *Combustion and Flame,* vol. 158, pp. 774-789, 2011.

[42] J. Hilliard and R. Wheeler, "Nitrogen Dioxide in Engine Exhaust," *SAE Transactions,* vol. 88, no. SAE 790691, pp. 2343-2354, 1979.

[43] E. Merryman and A. Levy, "Nitrogen Oxide Formation in Flames: The Roles of NO2 and Fuel Nitrogen," *Symposium (International) on Combustion,* vol. 15, no. 1, pp. 1073-1083, 1975.

[44] J. Tassitano, *NO2 Emissions from 2-Stroke Large Bore Natural Gas Engines*, (MS Thesis, Colorado State University), 2003.

[45] D. Olsen and J. Lisowski, "Prechamber NOx Formation in Low BMEP 2-Stroke Cycle Natural Gas Engines," *Applied Thermal Engineering*, vol. 29, no. 4, pp. 687-694, 2009.

[46] J. Hiltner and A. Loetz, "Fundamentals of NOx Formation in Pre-Chambered Equipped Gas Engines," in *11th Dessau Gas Engine Conference*, Dessau-Roßlau, Saxony-Anhalt, 2019.

[47] J. Gingrich, D. Olsen, P. Puzinauskas and B. Willson, "Precombustion chamber NOx emission contribution to an industrial natural gas engine," *International Journal of Engine Research*, vol. 7, no. 1, pp. 41-49, 2006.

[48] J. Klimstra and J. Westing, "NO2 from Lean-Burn Engines - On its Lower Sensitivity to Leaning than NO," *SAE Technical Paper Series*, no. 2, 1995.

[49] J. C. Hilliard and R. W. Wheeler, "Nitrogen Dioxide in Engine Exhaust," *SAE Transcations*, vol. 88, no. SAE 790691, pp. 2343-2354, 1979.

[50] P. Blumberg and J. Kummer, "Prediction of NO Formation in Spark-Ignited Engine - An Analysis of Methods of Control," *Combustion Science and Technology*, vol. 4, no. 1, pp. 73-95, 1971.

[51] R. R. Raine, C. R. Stone and J. Gould, "Modeling of Nitric Oxide Formation in Spark Ignition Engines with a Multizone Burned Gas," *Combustion and Flame*, vol. 102, no. 3, pp. 241-255, 1995.

[52] G. A. Lavoie and P. N. Blumberg, "A Fundamental Model for Predicting Fuel Consumption, NOx, and HC Emissions of the Conventional Spark-Ignited Engine," *Combustion Science and Technology,* vol. 21, no. 5-6, pp. 225-258, 1980.

[53] D. Baulch, D. Drysdale and D. Horne, Evaluated Kinetic Data for High Temperature Reactions, Vol. 2, London: Butterworth and Co. Ltd., 1973.

[54] G. Pirker, P. Mayr, J. Zelenka, M. Krenn, C. Redtenbacher and A. Wimmer, "Method for Analyzing Prechamber NOx Emissions from Large Gas Engines," in *28th CIMAC World Congress 2016*, Helsinki, 2016.

[55] J. Moore, "The Effects of Atmospheric Moisture on Nitric Oxide Production," *Combustion and Flame,* vol. 17, pp. 265-267, 1971.

[56] L. Dodge, J. Kubesh, D. Naegeli and P. Campbell, "Modeling NOx Emissions from Lean-Burn Natural Gas Engines," *SAE Technical Paper Series,* 1998.

[57] R. Corr, P. Malte and N. Marinov, "Evaluation of NOx Mechanisms for Lean, Premixed Combustion," *Journal of Engineering for Gas Turbines and Power,* vol. 114, pp. 425-434, 1992.

[58] A. Pundle, *Modeling and Analysis of Oxides of Nitrogen and Formaldehyde in Large-Bore, Lean-Burn, Natural Gas Engines,* (MS Thesis, University of Washington), 2013.

[59] J. Liu, H. Bommisetty and C. Dumitrescu, "Experimental Investigation of a Heavy-Duty Compression Ignition Engine Retrofitted to Natural Gas Spark Ignition Operation," *ASME Journal of Energy Resources Technology*, vol. 141, p. 112207, 2019.

[60] S. Christensen, K. Ajayi, D. Abata and K. Carlin, "An Experimental and Theoretical Study of Fuel Composition on Noxious Emissions in a Natural Gas Engine Operating on Wellhead Gas," in *ASME International Combustion Engine Division Fall Technical Conference*, 2015.

[61] M. Feist, M. Landau and E. Harte, "The Effect of Fuel Composition on Performance and Emissions of a Variety of Natural Gas Engines," *SAE Internationl Journal of Fuels and Lubricants*, vol. 3, no. 2, pp. 100-117, 2010.

[62] M. Graboski, R. McCormick, A. Newlin and D. Dunnuck, "Effect of Fuel Composition and Altitude on Regulated Emissions from a Lean-Burn, Closed Loop Controlled Natural Gas Engine," in *SAE Technical Paper 971707*.

[63] J. Ladd, B. Neuner and D. Olsen, "Variable Fuel Composition Air Fuel Ratio Control of Lean Burn Engines," Pipeline Research Council International, 2016.

[64] J. Miller and C. Bowman, "Mechanism and Modeling of Nitrogen Chemistry in Combustion," *Progress in Energy and Combustion Science*, vol. 15, no. 4, pp. 287-338, 1989.

[65] R. Hanson and S. Salimian, Combustion Chemistry, Berlin: Springer-Verlag, 1984.

[66] C. Bowman, R. Hanson, D. Davidson, W. Gardiner, V. Lissianski, G. Smith, D. Golden, M. Frenklach and M. Goldenberg. [Online]. Available: http://www.me.berkeley.edu/gri_mech/.

[67] G. P. Smith, D. Golden, M. Frenklach, N. Moriarty, B. Eiteneer, M. Goldenberg, C. Bowman, R. Hanson, S. Song, W. Gardiner, V. Lissianski and Z. Qin. [Online]. Available: http://www.me.berkeley.edu/gri_mech/.

[68] A. Dean and J. Bozzelli, Gas-Phase Combustion Chemistry, New York: Springer-Verlag, 2000.

[69] P. Glarborg, J. Miller, B. Ruscic and S. Klippenstein, "Modeling nitrogen chemistry in combustion," *Progress in Energy and Combustion Science,* vol. 67, pp. 31-68, 2018.

APPENDIX A

NO_2 PREDICTIONS

Using the full GRI mechanism also allowed for simulated values of engine-out NO_2. Accuracy of NO_2 predictions was not of importance for this work, but a brief analysis was performed to see how well the model could predict NO_2 for possible future improvements, if NO_2 accuracy becomes desirable. Figure 49 shows the simulated NO_2 values for the 10 nominal runs.

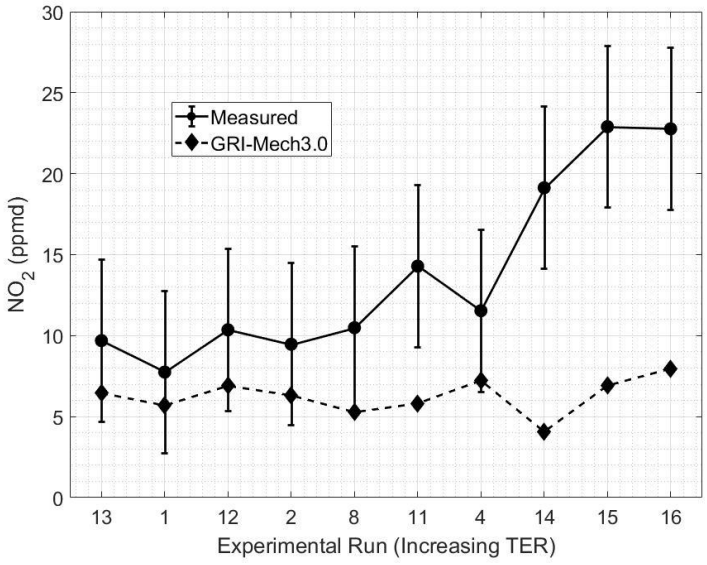

Figure 49: Measured and simulated NO_2 concentration when using full GRI-Mech3.0 for each nominal run.

Since total NO_x predictions using GRI-Mech3.0 are over predicted in general, it is perhaps more beneficial to look at the model's predicted NO_2/NO_x ratio since it is a better indicator of agreement with real engine behavior. Figure 50 shows the NO_2/NO_x ratios for the 10 nominal runs.

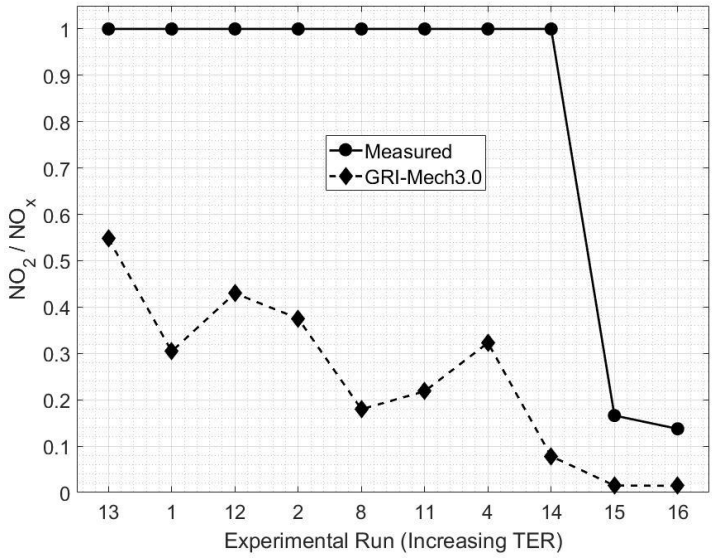

Figure 50: Measured and simulated NO_2/NO_x ratios for each nominal run.

Overall, it is observed that the model is able to produce a general downward trend in NO_2/NO_x ratio as TER increases. This suggests that the NO_2 kinetics may be reacting to the lower in-cylinder temperatures of the leaner cases, thereby destroying less NO_2. That said, predicted ratios still fall short of unity observed for the experimental data for TER values less than ~0.42 (Run-14). NO_2/NO_x ratios decrease for the two richest cases, though this is attributed mostly to the under prediction of NO_2, seen in Figure 49, and a severe over-prediction in total NO_x.

These results are to be expected and highlight the limitations of the model in capturing the in-cylinder effects which promote NO_2 survival. The lack of stratification and quenching regions makes for higher bulk in-cylinder temperatures which lead to less NO_2 than observed in experimental data. These drawbacks are a barrier to NO_2 accuracy, but do not affect the accuracy of total NO_x predictions.

APPENDIX B

CHEMKIN SI ENGINE SIMULATIONS

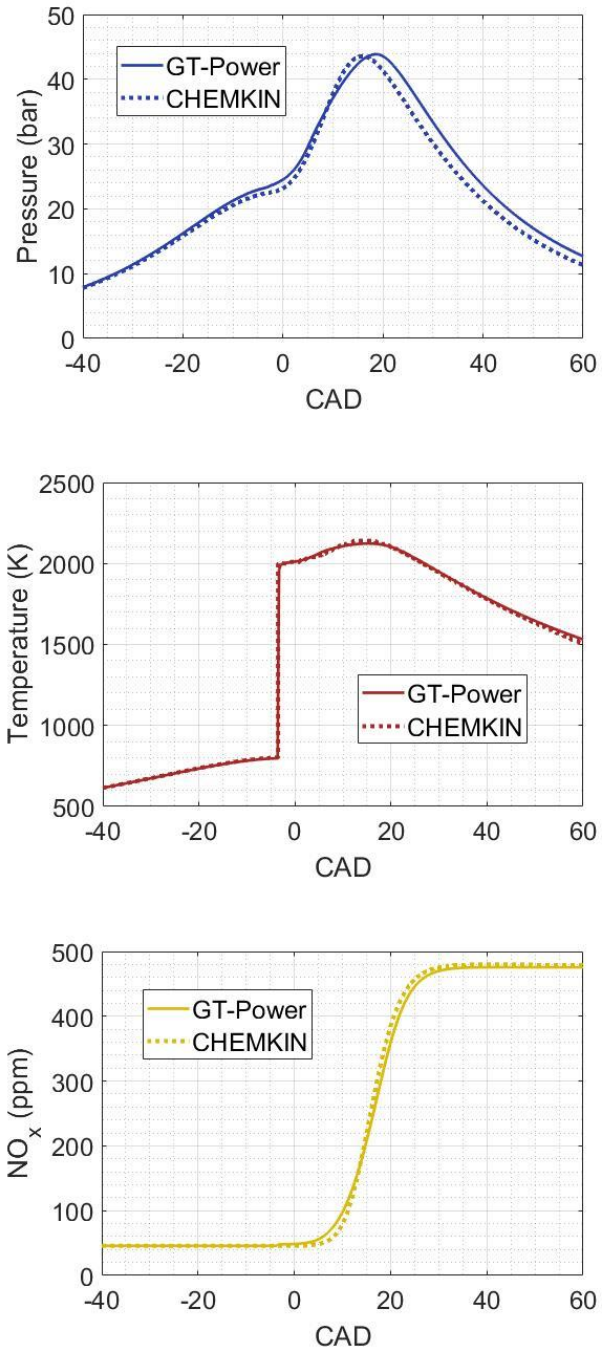

Figure 51: Pressure, Burned Zone Temperature, and NO_x profiles for Run-15.

APPENDIX C

REDUCED MECHANISM INVESTIGATION

Both GRI-Mech3.0 and the latest natural gas combustion mechanism from Glarborg et al. [69] were tried with mechanism reduction. CHEMKIN's SI module was again used to recreate pressure and burned temperature but this time for Run-4, which has a TER value nearest to the median TER value for the dataset. Each mechanism was used in the simulation, and then reduced.

Overall, results from mechanism reduction were promising, but did not lead to conclusions which greatly improved the prediction method. Each mechanism was reduced using relative allowable tolerances on both maximum NO concentration and maximum burned gas temperature. Tolerances of 10% for both mechanisms resulted in the removal of too many species such that, when used in GT-Power, no ignition was detected. The Glarborg mechanism was successfully reduced to 43 species from 151 with a 3% tolerance, but the number of reactions in the mechanism was still too great to be used in GT-Power. A 5% tolerance used with the GRI mechanism eliminated 15 species, but only removed just over one-third of the simulation time needed for each condition, resulting in a run time of 36 minutes.

Reducing mechanisms could be useful for future work on this model if more kinetic accuracy is desired. However, combustion mechanism use for predicting NO_x with GT-Power was abandoned for this work. Suitable accuracy was attained with the use of equilibrium combustion and a modified NO_x mechanism in a fraction of the time.